Transition Metal Carbides for Thermocatalytic Conversion of Carbon Dioxide via Reverse Water Gas Shift and Sabatier Reactions

by

Faisal Mohamed Khan

A thesis

presented to the University of Waterloo

in fulfillment of the

thesis requirement for the degree of

Master of Applied Science

in

Chemical Engineering

Waterloo, Ontario, Canada, 2018

Author's Declaration

I hereby declare that I am the sole author of this thesis. This is a true copy of the thesis, including any required final revisions, as accepted by my examiners.

I understand that my thesis may be made electronically available to the public.

Abstract

The conversion of carbon dioxide (CO_2) to synthetic fuels and chemicals is seen as a promising approach for reducing greenhouse gas emissions. Syngas (a mixture of CO and H_2) that can be obtained from CO_2 via the reverse water gas shift (RWGS) reaction can be further processed through the Fischer Tropsch process to produce higher hydrocarbons. Synthetic natural gas (CH_4) produced from the Sabatier reaction can help reducing consumption of fossil fuel and also can serve as an energy reservoir for renewable electricity via power-to-gas. However, utilization of the abovementioned reaction pathways is still limited due to various challenges including catalyst activity, selectivity, and stability. This thesis focuses on the development of catalytic materials for the RWGS and Sabatier reactions.

The first part of this thesis first focuses on a literature overview of recent developments in CO_2 conversion through the RWGS and Sabatier reaction. Then, the experimental setup, catalyst synthesis procedures, catalytic performance evaluation, and characterization techniques are outlined.

The second part discusses the results of the two transition metal carbides tested, namely molybdenum carbide (Mo_2C) and cobalt carbide (Co_2C). The catalytic performance of these catalysts was evaluated as a function of operation parameters for different synthesis procedures. The mechanisms of catalytic reactions are postulated and catalyst characterization results are provided.

To briefly outline the most important findings, the Mo_2C catalyst showed nearly complete selectivity towards CO formation at all temperatures tested, whereas the Co_2C

catalyst appeared to be highly selective towards CH_4 formation. The performance of the corresponding metal oxides are also evaluated to evaluate the effect of carburization on the performance of the catalyst. The transitions metal oxides of molybdenum and cobalt both showed a substantial improvement in both conversion and selectivity after the carburization process. The performance of the catalysts supported on Al_2O_3 at a 1:4 metal-to-support basis was also analyzed. During the stability tests of supported catalysts, CO_2 conversions of 84% and 74% were recorded over the Mo_2C and Co_2C catalysts, respectively, with a negligible drop in catalytic performance after 42 and 64 h time on stream.

Key words: CO_2 conversion, thermocatalytic conversion, reverse water gas shift, Sabatier reaction, molybdenum carbide, cobalt carbide

Acknowledgement

I would first like to thank my supervisor Professor David Simakov for his patience, continuous support and guidance throughout my Master's program.

I would also like to thank my committee members: Professor Boxin Zhao, Professor Aiping Yu for their valuable comments and suggestions on my research project.

This work would not have been possible without the help and advice from Yichen Zhuang, Robert Currie, Sogol Tabar, Guanjie Sun and Alex McGowan.

Last but not least, I would like to express my gratitude to my family and friends for their support and encouragement.

This project was funded by the Natural Science and Engineering Research Council (NSERC) of Canada through the NSERC Discovery Grant Program.

Table of Contents

List of Figures

List of Tables

Chapter 1

Introduction

1.1 Background

Climate change due to anthropogenic activities has been a topic of research interest due to its potential adverse impacts on everyday life. Reduction of greenhouse gases such as carbon dioxide, which forms a significant share of the overall greenhouse gas emissions, is seen as a vital step to mitigate the effects of climate change [1]. The current avenues explored to reduce atmospheric CO_2 levels include CO_2 sequestration, increasing contribution of renewable energy sources to the power grid and CO_2 utilization for processing new synthetic chemicals. Carbon sequestration, which involves the capture and storage of CO_2, is often limited by the overall financial cost of the project and high energy requirements [2]. Conversion of CO_2 into synthetic fuels and chemicals is an attractive alternative to CO_2 sequestration. Electrochemical and photocatalytic reduction, biological conversion and thermocatalytic reduction are the current pathways to produce synthetic chemical and fuels from CO_2.

Research in the electrochemical conversion of CO_2 is more focused on the production of fine chemicals such as urea and formate [3, 4]. This approach is promising but the potential impact on the atmospheric CO_2 levels is relatively small because of the limited market for fine chemicals. Photocatalytic and biological methods still require significant research to improve product yield and process efficiency. Thermocatalytic reduction is currently the most viable option as it is more advantageous in terms of kinetics and has higher product throughput [5]. The chemical products from thermocatalytic CO_2

hydrogenation can be categorized into three classes based on products, namely methanol, hydrocarbons, and carbon monoxide (CO) [6].

The reverse water gas shift reaction, Eq. (1), involving the reduction of CO_2 into CO, is an attractive option for CO_2 conversion as the syngas produced can be then used as a feedstock for either the Fischer Tropsch process, Eq. (2), or methanol synthesis, Eq. (3):

$$CO_2 + H_2 \rightleftarrows CO + H_2 \qquad \Delta H^{\circ}_{298} = 41 \text{ kJ/mol} \qquad (1)$$

$$(2n+1)H_2 + nCO \rightarrow C_nH_{2n+2} + nH_2O \qquad \Delta H^{\circ}_{298} = -162.50 \text{ kJ/mol} \qquad (2)$$

$$CO + 2H_2 \rightarrow CH_3OH \qquad \Delta H^{\circ}_{298} = -90.84 \text{ kJ/mol} \qquad (3)$$

The Sabatier reaction represented by Eq. (4), which is often accompanied by CO methanation Eq. (5), is seen as another possible avenue for CO_2 utilization for the production of synthetic natural gas, which can then be distributed through the existing natural gas infrastructure.

$$CO_2 + 4H_2 \rightleftarrows CH_4 + 2H_2O \qquad \Delta H^{\circ}_{298} = -164.9 \text{ kJ/mol} \qquad (4)$$

$$CO + 3H_2 \rightleftarrows CH_4 + H_2O \qquad \Delta H^{\circ}_{298} = -206.1 \text{ kJ/mol} \qquad (5)$$

Catalysts which have shown to have high activity for CO_2 hydrogenation are precious metals and group VIII transition metals (Co, Ni and Cu) [7, 8]. Although precious metals have excellent activity and stability, they are often not commercially viable due to high costs [7]. Group VIII transition metals find more application in commercial catalytic processes due to their low cost and reasonably high activity and as such, these catalysts are seen as an attractive option for CO_2 utilization [8].

Recently transition metal carbides have been explored as potential catalysts for CO_2 hydrogenation due to similarities in their electronic structures to those of precious metals, providing high catalytic activity in reforming [9], CO_2 hydrogenation [10,11], water gas shift reaction [12,13], and CO hydrogenation [14,15]. In particular, Mo_2C has been of particular interest due to its low cost and dual functionality for H_2 dissociation and CO_2 scission [16].

Research into other transition metal carbides were often limited due to the assumption that metal carbide species were either catalytically inactive or contributed to the deactivation of the catalyst [17]. Formation of metal carbide was often associated with the deactivation of catalyst in the Fischer Tropsch process with chain length assumed to reduce with formation of carbide species on the surface [18]. However, recent investigation into Co_2C for alcohol synthesis via the Fischer Tropsch process showed remarkable activity and selectivity. The activity of the catalyst was attributed to the non-dissociative CO adsorption similar to noble group metals, whereas Co is more active for dissociative CO adsorption and subsequent chain growth [19].

Research into these groups of catalytic materials is still lacking with only preliminary understanding of the mechanism involved. The catalytic hydrogenation of CO_2 for transition metal carbides is currently limited to research on Mo_2C with activity of other metal carbides yet to be explored. The effect of the preparation conditions on the activity is also not well understood often resulting in varied results for transition metal carbides prepared using different preparation procedures. Activation and deactivation mechanism of these catalysts also needs to be further explored.

1.2 Aims and objectives

The overall objective of this thesis is to develop suitable transition metal carbide catalysts for the RWGS and Sabatier reactions. The first goal is to achieve CO_2 conversions close to equilibrium values, selectivity above 90% (to either CO or CH_4), and good stability at elevated space velocities (high throughput). The second goal is to deduce reaction mechanisms and pathways.

The above mentioned objectives were achieved using the following methodology:

1. Conducting catalytic performance evaluation of Mo_2C and Co_2C catalysts in the RWGS and Sabatier reactions using a range of operating conditions (pressure, temperature, and feed rate).
2. Conducting catalytic performance evaluation of the corresponding metal oxides to investigate the effect of carburization (converting oxide to carbide) on the catalyst activity, selectivity, and stability.
3. Modifying the catalyst synthesis procedure to investigate the effects of preparation conditions on the catalyst performance under varying operating conditions.
4. Conducting catalyst characterization using analytical techniques (XRD, TEM etc.) and temperature programmed reactions to deduce possible reaction mechanisms.

Chapter 2

Literature review

2.1 The reverse water-gas shift reactions

The water gas shift reaction (WGS) was first discovered in 1888 [20]. This reaction produces hydrogen (H_2) and is currently used in large-scale industrial processes for the synthesis of ammonia. The reverse water gas shift (RWGS) reaction was initially considered as an undesirable reaction due to the formation of CO, which can affect some systems. As a result, catalyst for the WGS reaction were designed to work at low temperatures to avoid CO formation.

Recently, the RWGS reaction was considered as a key step in the utilization of CO_2 and estimated to be a more efficient way to produce liquid fuels as the process can be integrated with current technologies for thermocatalytic conversions [21]. In order to achieve high conversion for the RWGS reaction it should optimally be run at high temperatures due to the endothermic nature of the reaction and the high stability of CO_2. At higher temperatures, however, the reaction is limited by deactivation due to coking and sintering. The equilibrium can be shifted towards CO formation by changing feed composition. At high H_2:CO_2 feed ratio more CO_2 is consumed although this approach increases the operational cost associated with separation of H_2 from the product stream [22]. Other alternatives to shift the equilibrium include selective removal of the water being formed by using a desiccant bed or a membrane permselective to water [23].

2.1.1 Catalysts for the reverse water-gas shift reaction

Noble metal catalysts:

Noble metals such as Pt, Pd, and Rh supported on various supports such as Al_2O_3, ZrO_2, TiO_2, and CeO_2 have been found to be active for the RWGS reaction. 1% Pt/Al_2O_3 achieved 42% CO_2 at 875°C at a H_2:CO_2 of 3:2.1 and at a GHSV of 25,000 ml/(g h). The activity of the 1% Pt/Al_2O_3 was also tested against a 1% Pt/TiO_2 to understand the effect of the support on catalytic performance. The higher activity of the Pt/TiO_2 catalyst was explained as result of the formation Pt-O_v-Ti^{3+} site formed on the Pt/TiO_2 catalyst due to the reducible characteristics of the TiO_2 support [24]. Pettigrew et al. conducted studies on Pd on various supports (CeO_2, Al_2O_3, La_2O_3 and PrO_2) for the RWGS reaction. They have found that Pd supported on ceria showed higher reaction rates than the other supports due to strong metal-support interactions [25]. Goguet et al. suggested high CO concentration caused increasing carbon deposition on the catalyst surface by conducting temperature programmed oxidation (TPO) experiments on 2% Pt/CeO_2 catalyst [26]. CO_2 conversion over Pd-based membrane was found to achieve 10% at 723 K and H_2:CO_2=3, and operating pressure was found to have a strong impact on CO_2 conversion [27].

Transition metal catalysts:

Commercial WGS reaction catalysts are often studied for the RWGS reaction due to the reversibility of the reaction. Commercial WGS catalysts such as Cu/ZnO have good activity for the RWGS reaction. Due to its high selectivity to CO production, $CuO/ZnO/Al_2O_3$ was investigated as a catalyst for the RWGS reaction. Despite the

advantage of low cost of this catalyst, its activity and stability are poor, especially at high temperatures required for the endothermic RWGS reaction.

In order to extend the lifetime of the Cu-ZnO based catalysts, a substantial amount of work has been done on studying the effects of different supports on the catalytic performance. Al_2O_3, Ga_2O_3, ZrO_2 and Cr_2O_3 were all found to improve catalytic performance of Cu-ZnO. Al_2O_3 and ZrO_2 increased the catalytic activity by improving Cu nanoparticles dispersion, while Ga_2O_3 and Cr_2O_3 have been found to increase the specific activity per unit of Cu surface area. Stability of the Cu-ZnO catalyst can also been improved by adsorbing small amounts of colloidal silica on Cu-ZnO precipitate during preparation. An interesting fact is that this catalyst showed stability for 500 h for methanol synthesis [28].

Ni and Co have also been explored as active phases for the RWGS reaction but they are more selective towards CH_4 formation via the methanation reactions, Eqs (4, 5). Also, these catalysts are prone to deactivation by coking at high temperatures that can occur via the following reactions:

$$2CO \rightleftarrows C + CO_2 \qquad \Delta H^{\circ}_{298} = -173.3 kJ/mol \tag{6}$$

$$CO + H_2 \rightleftarrows C + H_2O \qquad \Delta H^{\circ}_{298} = -131.3 kJ/mol \tag{7}$$

Catalysts based on transition metal carbides:

Transition metal carbides are an attractive, low cost alternative, as their surfaces have electronic configurations similar to those of some precious metals, providing high catalytic activity in reforming [29], CO_2 methanation [30], water gas shift reaction [31-32], and CO

hydrogenation [33-34]. Molybdenum carbide (Mo_2C) is of particular interest due to its dual functionality for H_2 dissociation and CO_2 scission [35]. Mo_2C has been recently studied as a catalyst for the RWGS reaction [35-37]. The performance of the Mo_2C catalyst prepared by carburizing in C_2H_4 at 700 K in the RWGS reaction was found to be superior to Pt and Pd in terms of both conversion and selectivity [35]. In another work, Mo_2C nanowires synthesized via calcining the ammonium heptamolydate/aniline co-precipitate provided CO_2 conversion greater than 60% at 873 K and GHSV of 36,000 ml/(g h). The catalyst had 100% selectivity to CO at H_2:CO_2 molar ratio of 4. The selectivity to CO production was maintained for 20 h at 873 K at a space velocity of 240,000 ml/(g h) and H_2:CO_2 molar ratio of 1, although the conversion dropped to 28% [36].

While these recent findings are promising, further investigation is necessary to evaluate the applicability of Mo_2C as a catalyst for the RWGS reaction. In particular, it is required to study in more detail the Mo_2C-catalyzed RWGS reaction at high CO_2 conversions, which is more relevant to industrial applications. Recent studies mainly focus on the low temperature range when CO_2 conversion is less than 30% [37]. Also, it is necessary to investigate the catalytic performance in a wide range of space velocities and to analyze the extent of catalyst deactivation at high temperatures and over extended time on stream. More insight into the RWGS reaction mechanisms over Mo_2C is also required.

2.1.2 Mechanisms of the reverse water-gas shift reactions

The exact mechanism of the RWGS reaction is still being debated. The two commonly accepted mechanisms are the surface redox and the associative/formate decomposition mechanism. The surface redox mechanism occurs by the dissociative adsorption of CO_2 giving a surface bound CO and O atom. The H_2 present in the reaction mixture also

undergoes dissociative adsorption to form surface H species which then react with the O species present on the surface to form H_2O and CO_2 that desorbs from the surface. The reactions involved in the process can be summarized as follows [38]:

$$
\begin{aligned}
&CO_{2(g)} \rightleftarrows CO_a + O_a \\
&CO_a \rightleftarrows CO_{(g)} \\
&H_{2(g)} \rightleftarrows 2H_a \\
&H_a + O_a \rightleftarrows OH_a \\
&H_a + OH_a \rightleftarrows H_2O_a \\
&H_2O_a \rightleftarrows H_2O_{(g)}
\end{aligned}
\tag{8}
$$

Despite much research it still remains unclear as to the precise mechanism of OH_a formation. It is either the elementary step shown above in Eq. 8 or the H_2O catalyzed process shown in Eq. 9 [38].

$$
\begin{aligned}
&H_2O_a + O_a \rightleftarrows 2OH_a \\
&H_a + OH_a \rightleftarrows H_2O \\
&\text{Net: } \; H_a + O_a \rightleftarrows OH_a
\end{aligned}
\tag{9}
$$

Various mechanistic studies have been done on the Cu/ZnO catalyst for understanding steps involved in the formation of products. For the redox mechanism, the concept of the oxidation and reduction cycle was suggested. In this mechanism CO_2 was oxidized by Cu(0) to form CO and surface bound O. Gas phase H_2 dissociatively adsorbs on the catalyst

to form surface H that reacts with the bound O to form H_2O. The two species then desorb from the surface. H_2 from the feed acts as a reducing agent for the Cu_2O formed. Oxidation of the surface with CO_2 was determined to be the rate-determining step [39]. Redox mechanism is supported by the findings of Hadden et al. who showed that CO can be formed from CO_2 on the surface of Cu without the addition of any H_2 to the reactant gas mixture, whereas the formate mechanism cannot account for the CO formation in the absence of H_2 [40]. Kinetic studies conducted by Ernst et al. match well the experimental work further supporting the redox mechanism [38].

In the formate decomposition mechanism model, the CO is assumed to be formed as a result of the decomposition of formate intermediates formed as a result of association of CO_2 with H_2. Some researcher favor the formate decomposition mechanism. It has been reported that CO production rate increases with the concentration of formate species on Cu/SiO_2 catalyst, indicating the formation of formate species play an important role in CO formation [41]. The mechanism is summarized as follows [42]:

$$
\begin{aligned}
&H_{2(g)} \rightleftarrows 2H_a \\
&CO_{2(g)} + H_a \rightleftarrows HCOO_a \\
&HCOO_a \rightleftarrows CO_a + OH_a \\
&OH_a + H_a \rightleftarrows CO_a + OH_a \\
&OH_a + H_a \rightleftarrows H_2O_a \\
&H_2O_a \rightleftarrows H_2O_{(g)}
\end{aligned}
\qquad (10)
$$

Rate expressions based on the formate mechanism tend to fit well experimental results in a majority of cases [42], whereas the redox-based kinetics typically cannot be used to explain the observed behavior [41]. In order to explain the limitations of both mechanisms, it has been suggested that both can occur simultaneously [40]. Another suggested mechanism involves the formation of carbonate species which then reacts with surface H to from CO and surface hydroxide species [43-44]. The mechanism is summarized as follows [44]:

$$
\begin{aligned}
&2OH^-_a \rightleftarrows H_2O_{(g)} + O^{2-}_{(a)} \\
&CO_{2(g)} + O^{2-}_a \rightleftarrows CO_3^{2-}_a \\
&CO_3^{2-}_a + H_{2(g)} \rightleftarrows CO_a + 2OH^-_a \\
&H_{2(g)} \rightleftarrows 2H_a \\
&O_a + 2H_a \rightleftarrows H_2O_a \\
&OH_a + H_a \rightleftarrows H_2O_a
\end{aligned}
\qquad (11)
$$

This hypothesis is still unproven as there is no enough evidence supporting it. Some studies, e.g., a study of Pt/CeO_2 by Goguet et al. support this mechanism. The rate determining step in their work was found to be the formation of a reaction intermediate not involving the presence of H, most likely a carbonate [45].

2.2 Sabatier reaction (CO_2 methanation)

The Sabatier reaction represented by Eq. (4) is seen as a possible avenue for CO_2 utilization for the production of synthetic natural gas (SNG), sometimes called renewable

natural gas (RNG), which can then be distributed through the existing natural gas infrastructure [46]. The reaction is highly exothermic and is typically accompanied by the RWGS reaction and CO methanation, Eqs (1, 5).

The Sabatier reaction has also been proposed as a method to upgrade landfill gas although the economic feasibility of this approach is still being investigated [47]. This reaction was also considered as a method to store excess energy from renewable energy sources by the power to gas process [48]. In addition, The National Aeronautics and Space Administration (NASA) has identified the Sabatier reaction as an important process for future manned space colonization of mars [49-50].

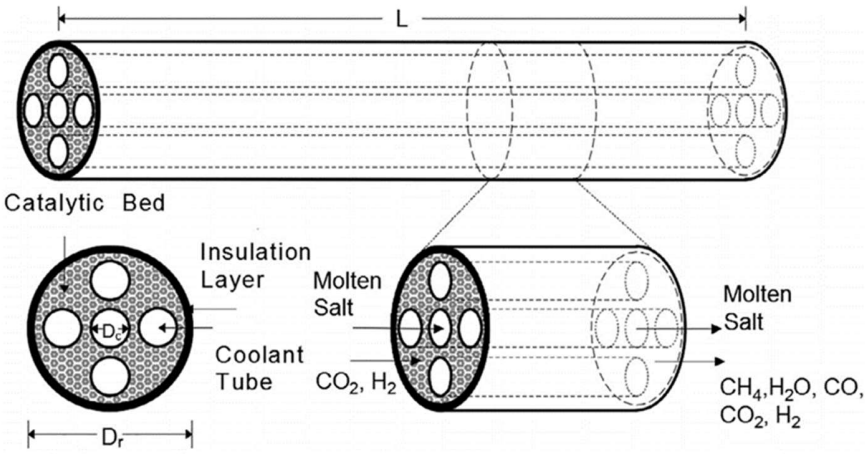

Figure 1: Sabatier reactor design with molten salt cooling [5].

CO_2 methanation is a thermodynamically favorable process ($\Delta G°_{298} = -164.9$kJ/mol). However, the reaction requires a suitable catalyst to overcome the kinetic limitation associated with reducing CO_2 to CH_4. The Sabatier reaction favors low temperatures and high pressures, although it is challenging to attain equilibrium conversions at lower temperatures. On the other hand, higher temperature operation leads to the deactivation of

catalyst through coking and sintering. To maintain the reactor at relatively low temperature, proper cooling is required for the Sabatier reactor. A new reactor design for Sabatier reaction was proposed, Fig. 1. The simulation results indicated that the heat removal was efficient thus CH_4 production could be maximized and catalyst deactivation could be further suppressed [51].

2.2.1 Catalysts for the Sabatier reaction

Ni based catalysts:

Ni based catalysts are the most commonly studied catalysts for the Sabatier reaction, due to low cost and good activity [52]. CO_2 conversion and CH_4 selectivity of 20 wt% Ni/Al_2O_3 catalyst are around 81% and 96% respectively under 400°C and 55,000 h^{-1} [53]. Al_2O_3 based supports are most commonly used for Ni catalyst due to the strong interaction between Ni and Al_2O_3 leading to the formation of mixed oxides such as $NiAl_2O_4$ which can prevents the reduction of Ni and hence improves catalytic performance [54].

The effect of metal loading was studied by Kester et al. who showed that Ni and Al_2O_3 interact to form two different active sites for methanation, one consisting of Ni crystallites and the other of mixed Ni and Al_2O_3. The mixed Ni and Al_2O_3 sites reduces with increased metal loading [54]. Mengdie et al. studied the addition of ZrO_2 to Ni supported on Al_2O_3. The ZrO_2 was found to improve the activity and stability of the catalyst by improving the dispersion of Ni and preventing the formation of mixed Ni-Al_2O_3 [55].

Supports such as SiO_2 and MgO were also studied showing generally good performance when operated for short durations [56-57]. Despite the abovementioned advantages, the implementation of Ni-based catalysts for CO_2 methanation is limited

because of high tendency to deactivation by poisoning, coking and sintering [58]. Poisoning of Ni catalysts typically occurs due to the presence of sulphur compounds in the feed gas stream [58, 59]. Sintering also plays an important role in the deactivation of Ni-based catalysts. Studies have indicated that Ni sintering proceeds by chemical sintering, via the formation of $Ni(CO)_4$ [60].

While operating at relatively low temperatures typically employed in CO_2 methanation (700-800 K) and in the absence of sulphur (can be removed from feed gas by adsorbents), catalytic activity of Ni is mainly reduced by coking. Carbon deposition deactivates the catalyst by fouling the catalyst surface, blocking catalyst pores and disintegrating the catalyst support [58]. The three major forms of carbon deposited on Ni catalysts are encapsulating hydrocarbons films formed by polymerization at temperatures below 750 K, whiskerlike carbon formed at temperatures higher than 725 K, and pyrolytic carbon formed by cracking of hydrocarbons above 875 K [58]. The most thermodynamically probable reactions involved in carbon deposition in the methanation process are CH_4 cracking, Eq. (12), Boudouard reaction, Eq. (6), and CO reduction (reverse gasification), Eq. (7) [61]:

$$CH_4 \rightleftarrows C + 2H_2 \qquad \Delta H^{\circ}_{298} = +74.8 \text{ kJ/mol} \qquad (12)$$

Noble metal based catalysts:

Ru has the highest catalytic activity for the Sabatier reaction. CO_2 conversion of 100% with almost complete selectivity towards the Sabatier reaction were achieved for 0.8wt% Ru/TiO_2 at a H_2/CO_2=4, P =0.1MPa at 160°C at a GHSV of 0.24 ml/(g s) [62]. 5wt% Ru/Al_2O_3 showed CO_2 conversion of 55% and CH_4 selectivity of 95% at 350°C and H_2:CO_2 = 3 [63]. When the effect of Ru loading ranging from 0.1-5wt% on Al_2O_3 were

tested. The high dispersion found at lower metal loadings improved selectivity towards CO [64].

Apart from Ru, other noble metals such as Pt and Pd have also shown good activity towards the Sabatier reaction [65-66]. Solymosi et al. tested the performance of various noble metals and arranged the activity of the metals in the following order: Ru > Rh ~Ir ~ Pd [67]. Lizuka et al. tested the performance of Rh on various catalyst supports. Rh supported on ZrO_2 had the highest CO_2 conversions at 85% at 240°C at a CO_2:H_2=1/10 and GHSV=36,000 h^{-1}. Rh supported on Al_2O_3 and SiO_2 showed only 40.6% and 19% CO_2 conversion at the same operating conditions. The higher activity of the Rh/ZrO_2 was associated with the faster dissociation of CO intermediates on the surface as compared to other supports [68].

Transition metal carbides:

Molybdenum carbide (Mo_2C) is currently the most intensively researched metal carbide for the hydrogenation of CO_2 due to its low cost and dual functionality for H_2 dissociation and CO_2 scission [35]. However, Mo_2C is more active for the RWGS reaction with methane being formed more as a side product. Research into other transition metal carbides was often limited due to the assumption that metal carbide species were either catalytically inactive or contributed to the deactivation of the catalyst [69]. Formation of metal carbide was often associated with the deactivation of catalyst in the Fischer Tropsch process with chain length assumed to reduce with formation of carbide species on the surface. However, reduction of Co_2C in H_2 after carburization was found to significantly increase activity of cobalt catalysts in the Fischer Tropsch process due to changes in the

crystalline structure of the material facilitated by the carburization of Co metal [70]. Recent investigation into Co_2C for alcohol synthesis via the Fischer Tropsch process showed remarkable activity and selectivity. The activity of the catalyst was attributed to the non-dissociative CO adsorption similar to noble group metals, whereas Co is more active for dissociative CO adsorption and subsequent chain growth [71].

2.2.2 Mechanisms of the Sabatier reaction

The mechanism for CO_2 methanation is considered to generally follow two pathways. The first pathway involves the reduction of CO_2 to CO (RWGS), followed by the methanation of CO [72,73]:

$$\begin{aligned} CO_{2(g)} &\rightleftarrows CO_a + O_a \\ CO_a &\rightarrow C_a + O_a \\ 2CO_a &\rightarrow C_a + O_a \\ C_a + H_a &\rightarrow CH_a \\ CH_a + H_a &\rightarrow CH_{2,a} \\ CH_{2,a} + 2H_a &\rightarrow CH_{4,g} \end{aligned} \tag{13}$$

For the first pathway the CO intermediate may either undergo hydrogenation to CH_x species as seen on Ru/TiO_2 or proceed to form surface carbon which is consequently hydrogenated to form CH_4 as in the case Ni Catalysts [76,77]. The second pathway involves the direct reaction of CO_2 and H_2 at the catalyst surface without the formation of the CO intermediate [74,75]:

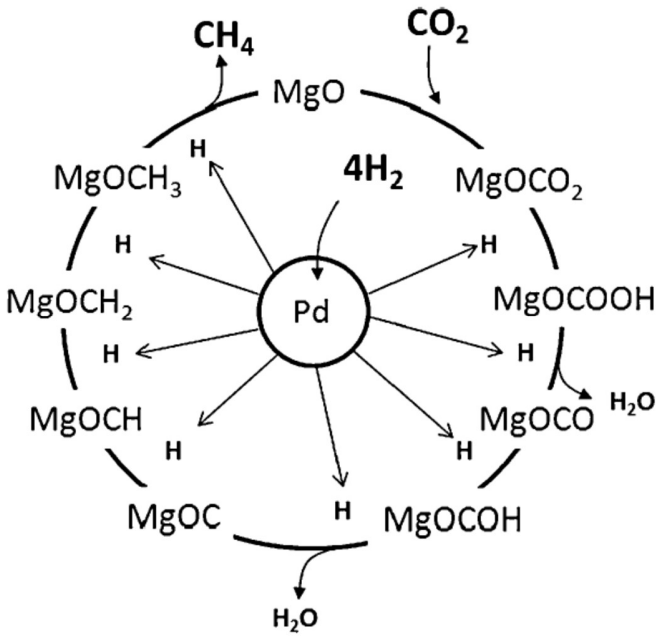

Figure 2:CO_2 hydrogenation over Pd-MgO [78].

Catalysts such as Pd-MgO_2 seem to follow the second pathway were the CO_2 reacts to form a surface carbonate and residual carbon species. The Pd then hydrogenates the surface carbonate species by supplying dissociated hydrogen at the surface [78].

Chapter 3

Experimental setup

3.1 Catalyst synthesis

Molybdenum carbide catalyst:

21.25wt% $Mo_2C/\gamma\text{-}Al_2O_3$ was synthesized using ammonium heptamolybdate tetrahydtrate (99% $(NH)_4Mo_7O_{24}\times 4\ H_2O$, Alfa Aesar) and commercial $\gamma\text{-}Al_2O_3$ support (250 m^2/g $\gamma\text{-}Al_2O_3$, Alfa Aesar) as precursors. The $\gamma\text{-}Al_2O_3$ support was crushed and sieved into particles (250-425 μm) and added to the $(NH)_4Mo_7O_{24}\times 4H_2O$ solution in deionized water adjusting for a 1:4 weight ratio of Mo:$\gamma\text{-}Al_2O_3$. The resulted slurry was stirred for 2 h and dried at 80°C overnight. The precipitate was calcined at 500°C for 4 h to produce $MoO_3/\gamma\text{-}Al_2O_3$.

To synthesize $Mo_2C/\gamma\text{-}Al_2O_3$, the supported MoO_3 was carburized in a quartz tube under the flow of H_2:CH_4 with a molar ratio of 4:1 (500 ml/min total flow rate). The heating rate was 10°/min for 20-150°C and 1°/min for 150-800°C. The sample was then held at 800°C for 2 h under the same H_2:CH_4 flow followed by reduction in H_2 (100 ml/min) for 1 h and cooling down to room temperature under N_2 (500 ml/min). Low temperature carburization was carried out using a H_2:C_2H_6 mixture (9:1, 500 ml/min) with a heating rate of 10°/min for 20-250°C and 1°/min for 250-650°C. The sample was then held at 650°C for 2 h, reduced in H_2 (100 ml/min) for 1 h and cooled down to room temperature under N_2 (500 ml/min). Bulk Mo_2C was prepared using the identical procedure excluding

the addition of γ-Al_2O_3, using either H_2:CH_4 or H_2:CH_4 for carburization (as described above).

Cobalt carbide catalyst:

22wt% Co_2C/γ-Al_2O_3 was prepared by dissolving cobalt (II) nitrate hexahydrate ($Co(NO_3)_2.6\ H_2O$) in deionized water. Crushed and sieved γ-Al_2O_3 was then added to this solution in a 1:4 weight ratio of Co:γ-Al_2O_3. The solution was stirred using a magnetic stirrer for 2 h. After stirring, the solution was dried at 80°C overnight. The residue was then collected and calcined in a furnace at 550°C for 4 h to produce 25.42% CoO_x/γ-Al_2O_3. 25.42% CoO_x/γ-Al_2O_3 is then carburized in a quartz tube in either a high temperature carburization mixture of hydrogen/methane in a molar ratio of 4:1 or in a low temperature carburization mixture of hydrogen/ethane in a molar ratio of 9:1.

High temperature carburization is carried at a flow rate of 0.5 L /min at a heating rate of 10°C/min from 20°C to 250°C followed by a heating rate of 1°C/min from 250°C to 800°C. The sample was then held at this temperature for 2 h. The catalyst was then cooled to room temperature under nitrogen. Low temperature carburization was carried out at a total flow rate of 0.5 L/min in a hydrogen/ethane mixture of 9:1 at a heating rate of 10°C min from 20°C to 250°C followed by a heating rate of 1°C/min from 250°C-650°C. The

sample was then held at this temperature for 2 h followed by reduction in hydrogen for 1 h. The catalyst was then cooled to room temperature in nitrogen flow.

3.2 Flow system setup

The experimental setup for catalytic performance evaluation is shown in Fig. 2. The CO_2 and H_2 fed to the reactor was controlled by two mass flow controllers. A 1/4″ stainless steel union tee (Swagelok) was used as a reactor, which was connected to a 1/4″ stainless steel tubing on both sides (Swagelok). The temperature inside the reactor was measured with a type K type thermocouple (1/8″, Omega Engineering, Inc.) which was placed in a direct contact with the catalytic bed. The catalyst was loaded into the reactor through the remaining tee opening, with quartz wool placed above the catalyst that was consequently sealed with a plug (Swagelok).

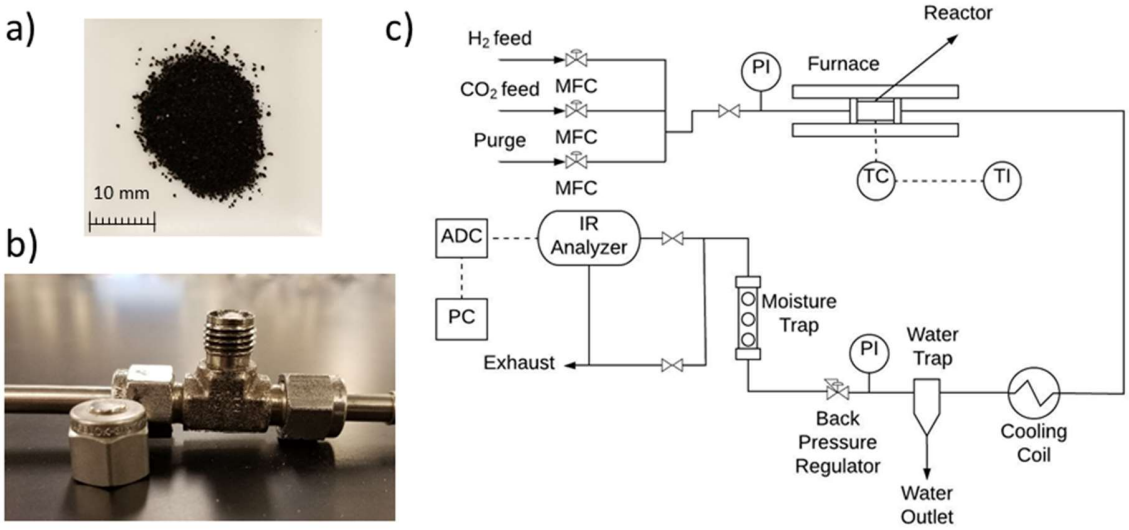

Figure 3: Flow system setup for catalytic performance evaluation.

The reactor was placed in a furnace (Lindberg/Blue M™ Mini-Mite™, Thermo Fisher Scientific) with the tee containing the catalyst being in the middle of the furnace. The temperature was controlled with a furnace built-in temperature controller (UP150, Yokogawa) using the thermocouple installed within the reactor (in contact with the catalytic bed). A back pressure regulator (S01094789B, Swagelok) was used to adjust pressure, Fig. 1b. Water was removed from the outlet stream using a mist trap (AFM40-N02-Z-A, SMC Corporation) before the back pressure regulator and a moisture trap column (5182-9411, Agilent Technologies, the original adsorbent was replaced with an orange silica gel, Fisher Scientific) downstream. Concentrations of CO, CO_2 and CH_4 in the outlet stream were measured on a dry basis with an IR analyzer (IR-208, Infrared Industries, Inc., USA) and continuously recorded using an analog-to-digital converter (USB 6008, National Instruments) and LabVIEW (National Instruments).

3.3. Catalyst characterization

Catalyst composition was verified using inductively coupled plasma mass spectrometry (ICP-MS, Prodigy SPEC). An ICP-MS consists of a high-temperature ICP (Inductively Coupled Plasma) source with a mass spectrometer. The ICP source is used to convert the atoms of the elements in the sample to ions. These ions are then separated and detected by the mass spectrometer. The sample is typically introduced into the ICP plasma as an aerosol, either by aspirating a liquid or dissolved solid sample into a nebulizer or by using a laser to directly convert solid samples into an aerosol. The sample aerosol once introduced into the ICP torch is completely desolvated and the elements in the aerosol are converted first into gaseous atoms and then ionized towards the end of the plasma.

For coupling to mass spectrometry, the ions from the plasma are extracted through a series of cones into a mass spectrometer, usually a quadrupole. The ions are separated on the basis of their mass-to-charge ratio and a detector receives an ion signal proportional to the concentration. The concentration of a sample can be determined through calibration with certified reference material such as single or multi-element reference standards.

Specific surface area (SSA) was measured with a Gemini VII 2390 surface area analyzer (Micromeritics Instrument Corporation) using N_2 as adsorption gas. The surface area analyzer uses nitrogen as a probing gas as it does it does not chemically react with the adsorbent. The analysis is generally conducted at the boiling point of nitrogen at 77K. The surface area analyzer calculates the specific surface area using the BET equation.

$$\frac{1}{v\left(p_0 / p\right)-1}=\frac{c-1}{v_m c}\left(\frac{p}{p_0}\right)+\frac{1}{v_m c} \tag{14}$$

Where p and p_0 are equilibrium pressures and saturation pressures of the adsorbates at the temperature of adsorption. v is the adsorbed gas quantity and v_m is the monolayer adsorbed gas quantity. c is the BET constant.

X-ray diffraction (XRD) patterns were acquired with a D8 Discover diffractometer (Bruker). X-ray diffraction works on the constructive interference of monochromatic X-rays and a crystalline sample. A cathode ray tube is used to generate X-rays which are, filtered to produce monochromatic radiation, collimated to concentrate, and directed toward the sample. The incident rays interacts with the sample producing constructive interference (and a diffracted ray) when conditions satisfy Bragg's Law ($n\lambda=2d\sin\theta$). This law relates the wavelength of electromagnetic radiation to the diffraction angle and the

lattice spacing in a crystalline sample. These diffracted X-rays are then detected, processed and counted. By scanning the sample through a range of 2θangles, all possible diffraction directions of the lattice should be attained due to the random orientation of the powdered material. Conversion of the diffraction peaks to d-spacings allows identification of the mineral because each mineral has a set of unique d-spacings. Typically, this is achieved by comparison of d-spacings with standard reference patterns.

To determine the extent of coking, thermal gravimetric analysis (TGA) was performed with a Q500 analyzer (TA Instruments) using a 5°/min heating rate under a flow of air (40 ml/min). Thermogravimetric analysis is a type of thermal analysis where the mass of the substance is measured over time as a function of temperature change. To analyze corresponding consumption/release of gases (O_2, CO_2, CO), temperature-programmed oxidation (TPO) was carried out using the flow system shown in Fig. 1 (2°/min heating rate, 200 ml/min air). Temperature-programmed reduction (TPR) was performed using the same flow system (10°/min heating rate, 200 ml/min H_2) with the outlet analyzed by Fourier-transform infrared spectroscopy (FTIR) with a MultiGas 2030 continuous gas analyzer (MKS Instruments). Prior to H_2 TPR, all samples were exposed to CO_2 (20-800°C, 10°/min, 200 ml/min CO_2).

3.4. Catalytic performance evaluation

The performance of the catalyst was evaluated at different temperatures and GHSV. Fresh catalyst was loaded into the reactor and reduced at 450°C before every test was performed. The reaction conditions for the performance test are listed as follows: (a) T=250-500°C, P=30 psi, H_2:CO_2=4, total flow rate=0.5 L/min; (b) T=450°C, P=30 psi,

H_2:CO_2=4, total flow rate=0.1-1.8 L/min. The reaction conditions of varying temperatures and GHSV are (a) and (b) respectively. The stability test were performed at 800°C for each catalyst at a GHSV of 100,000 ml/(g h), P=30psi, H_2:CO_2=4 and total flow rate of 0.5L/min.

CO_2 conversion and CO selectivity were calculated using Eq. (15) and Eq. (16):

$$X_{CO_2} = \frac{y_{CO} + y_{CH_4}}{y_{CO_2} + y_{CO} + y_{CH_4}} \tag{15}$$

$$S_{CO} = \frac{y_{CO}}{y_{CO} + y_{CH_4}} \tag{16}$$

Where y_{CO_2}, y_{CO} and y_{CH_4} are the fraction of each gas in the outlet measured by IR analyzer. Water was excluded from calculation since the humidity in gas was removed before analysis. GHSV is calculated by Eq. (17):

$$GHSV = \frac{Q_f}{w_c} \times 1000 \times 60 \tag{17}$$

Q_f is the feed flow rate and w_c is the catalyst weight loaded in the reactor. Carbon balance is defined as the total amount of carbon flown in the reactor divided by the amount of carbon dioxide flown out of the reactor, and were calculated using Eq. (18):

$$CB = (y_{CO_2} + y_{CO} + y_{CH_4})(1 + \alpha - f_1 - 4f_2) \tag{18}$$

In Eq. (18), α, f_1, and f_2 stand for H_2:CO_2 ratio in the feed, conversion to CO, and conversion to CH4, as defined in Eqs (19a-c) below ($F_{C,out}$ is the total outlet carbon-based molar flow rate):

$$\alpha = \frac{F_{H_2,f}}{F_{CO_2,f}} \tag{19a}$$

$$f_1 = \frac{y_{CO}}{(y_{CO_2} + y_{CO} + y_{CH_4})} = \frac{F_{CO,out}}{F_{CO_2,feed}} \tag{19b}$$

$$f_2 = \frac{y_{CH_4}}{(y_{CO_2} + y_{CO} + y_{CH_4})} = \frac{F_{CH_4,out}}{F_{CO_2,feed}} \tag{19c}$$

Eq. (19) above is obtained from the carbon balance definition, Eq. (19d), using Eq. (19e) to define the total outlet molar flow rate ($F_{CO,out}$ and $F_{CH_4,out}$ in Eq. (19e) correspond to the H_2 consumption in the RWGS and Sabatier reactions, Eqs (1, 4)):

$$CB = \frac{(y_{CO_2} + y_{CO} + y_{CH_4})F_{t,out}}{F_{CO_2,f}} \tag{19d}$$

$$F_{t,out} = F_{CO_2,f} + F_{H_2,f} - F_{CO,out} - 4F_{CH_4,out} \tag{19e}$$

Chapter 4

Results and discussion

4.1 RWGS reaction

4.1.1 Reverse water gas shift equilibrium

Because the reverse water gas shift reaction, Eq. (1), is reversible, the maximum conversion will be limited by equilibrium and will be a function of temperature. The equilibrium conversion can be evaluated analytically [79]. By first defining the total conversion and H_2/CO_2 feed ratio as in Eq. (20), expressions for the extent of each species at equilibrium can be derived (assuming no CH_4 formation), Eq. (21).

$$f_1 = \frac{n_{CO_2,f} - n_{CO_2,eq}}{n_{CO_2,f}}$$
$$\alpha = \frac{n_{H_2,f}}{n_{CO_2,f}} \tag{20}$$

$$\phi_{CO_2} = 1 - f_1$$
$$\phi_{H_2} = \alpha - f_1$$
$$\phi_{CO} = f_1$$
$$\phi_{H_2O} = f_1 \tag{21}$$

Equilibrium partial pressures can then be defined using the equilibrium extents derived above (y_i and P are mole fraction and total pressure, respectively):

$$P_i = y_i P = \left(\frac{\phi_i}{\sum \phi_j} \right) P$$
$$P_{CO_2} = \frac{1 - f_1}{1 + \alpha} P$$
$$P_{H_2} = \frac{\alpha - f_1}{1 + \alpha} P \tag{22}$$
$$P_{CO} = \frac{f_1}{1 + \alpha} P$$
$$P_{H_2O} = \frac{f_1}{1 + \alpha} P$$

These equilibrium partial pressures can then be substituted into the reverse water gas shift equilibrium constant:

$$K_{RWGS} = A_{RWGS} \exp\left(\frac{-\Delta H^\circ_{RWGS}}{R_g T} \right) = \frac{P_{CO} P_{H_2O}}{P_{CO_2} P_{H_2}} = \frac{f_1^2}{(1 - f_1)(\alpha - f_1)} \tag{23}$$

The final equation to be solved is given as follows:

$$A_{RWGS} \exp\left(\frac{-\Delta H^\circ_{RWGS}}{R_g T} \right) = \frac{f_1^2}{(1 - f_1)(\alpha - f_1)} \tag{24}$$

Note that the equilibrium conversion will be dependent on temperature as well as H_2/CO_2 feed ratio, but will not be dependent on pressure, since there is no change in number of moles, Eq. (1). The solution of Eq. (24) using known parameters is shown in Fig. 3 [80]. It is clear that temperature has the most significant effect on equilibrium conversion, though at higher temperatures ratio starts to have a more substantial impact. This substantiates the need for catalysts stable at high temperatures as below 700°C, it would be challenging to even reach 70% conversion.

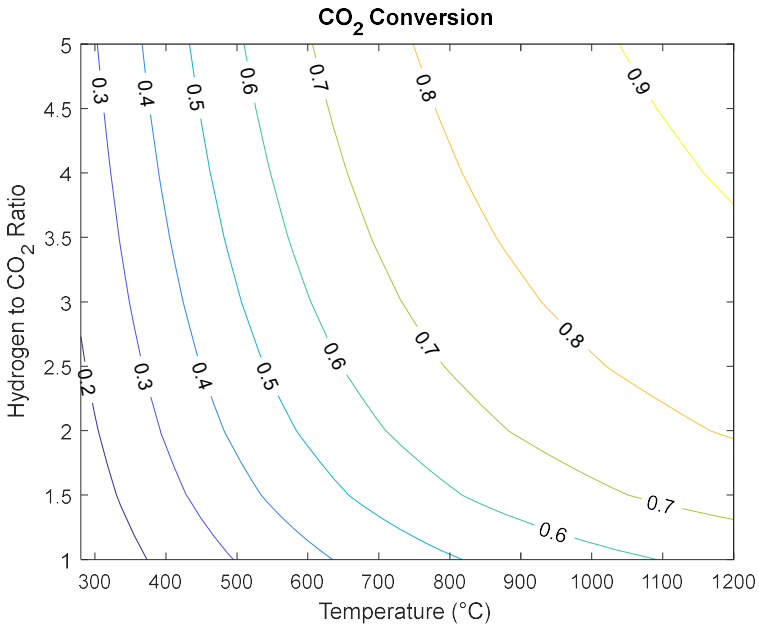

Figure 4: Equilibrium CO_2 conversion as a function of temperature and feed H_2:CO_2 ratio.

4.1.2 Catalytic performance of bulk and supported Mo_2C and MoO_3

The performance of both bulk and supported MoO_3 and Mo_2C were first tested at GHSV of 36,000 ml/(g h), P=3 bar and H_2:CO_2=4. The conversion profiles for the catalysts were similar at low GHSV velocities with variations occurring in the selectivity towards CH_4. The supported and unsupported MoO_3 showed a sharp increase in CH_4 selectivity at temperatures ranging from 450-600°C. The carbide remained relatively stable in terms of selective towards the RWGS reaction with bulk Mo_2C showing complete selectivity towards the RWGS at all temperatures tested. The catalyst all reached close to equilibrium conversion with oxides having approximately 10% lower conversion at 700°C.

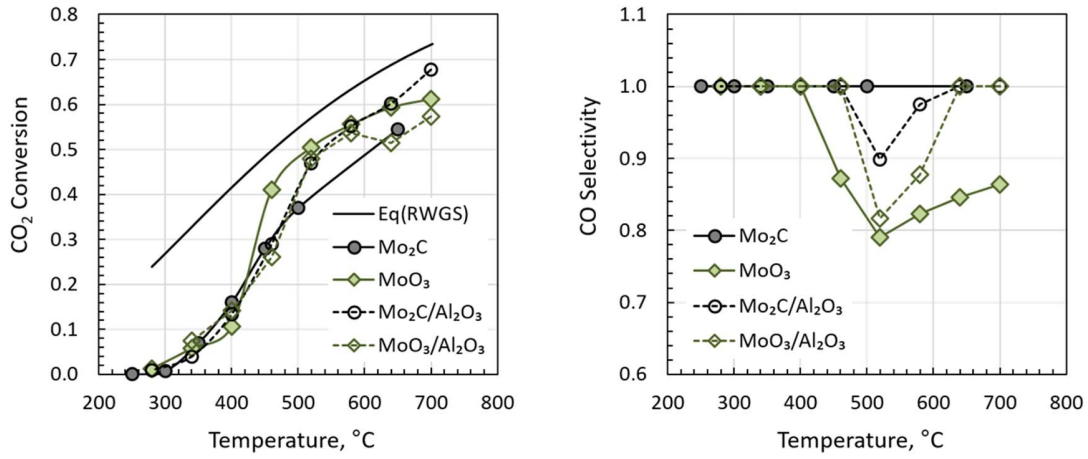

Figure 5: Catalytic performance of supported and bulk MoO_3 and Mo_2C at varying temperatures, GHSV=36,000 ml/(g h), P=30 psi, H_2:CO_2=4

4.1.3 Effect of carburization temperature on bulk Mo_2C

The performance of Mo_2C carburized at different temperatures and reaction mixtures are shown Figs 4, 5. High T-Mo_2C (high temperature carburization) showed complete selectivity towards the RWGS reaction at all temperatures tested. The conversion increased exponentially beyond 300°C for high T-Mo_2C and low T-Mo_2C (low temperature carburization). The maximum conversions recorded were 38% and 56% for the high T- and low T-Mo_2C respectively at 500°C and 30 psi. Although the low T-Mo_2C had higher overall conversion, it showed high selectivity towards the methanation reaction at T > 300°C.

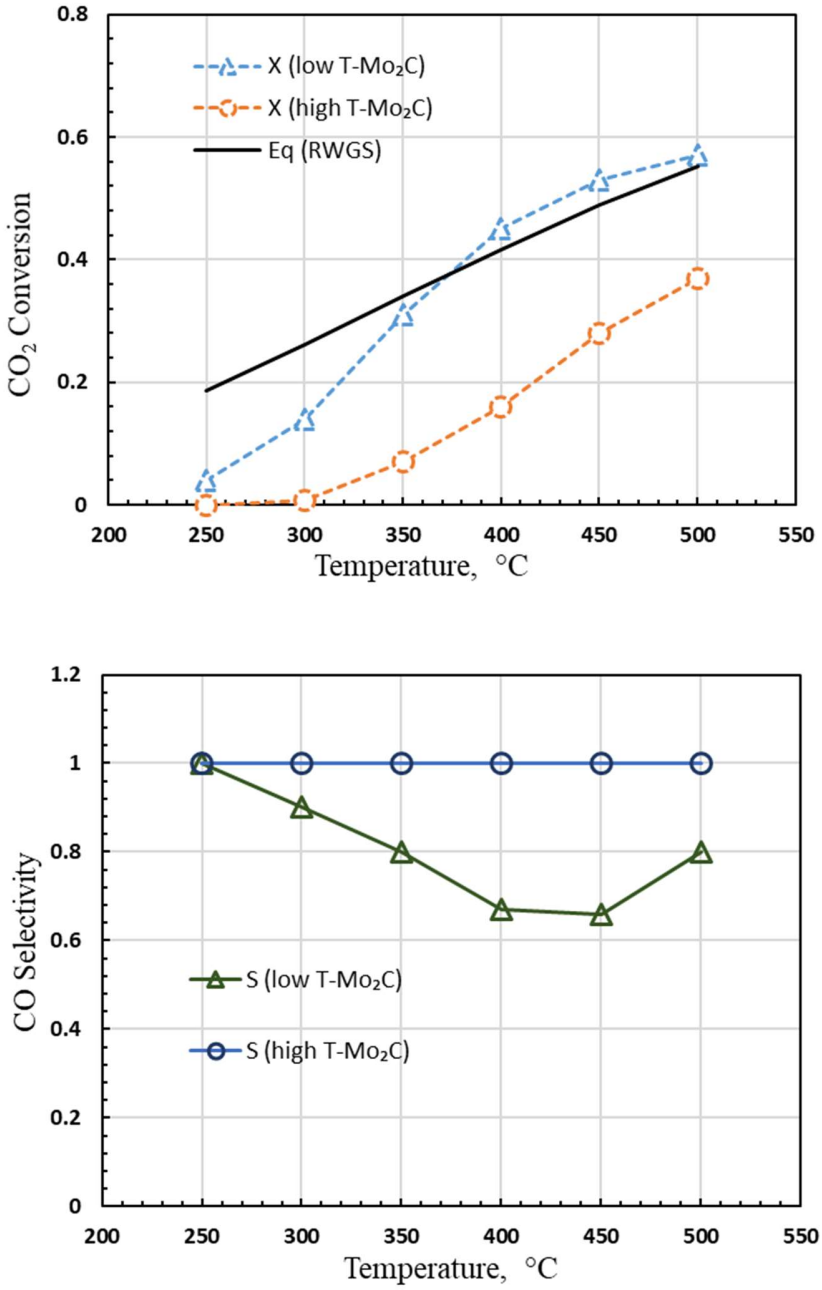

Figure 6: Performance of low T-Mo_2C and high T- Mo_2C at varying temperatures, GHSV=100,000 ml/(g h), P =30 psi, H_2:CO_2=4

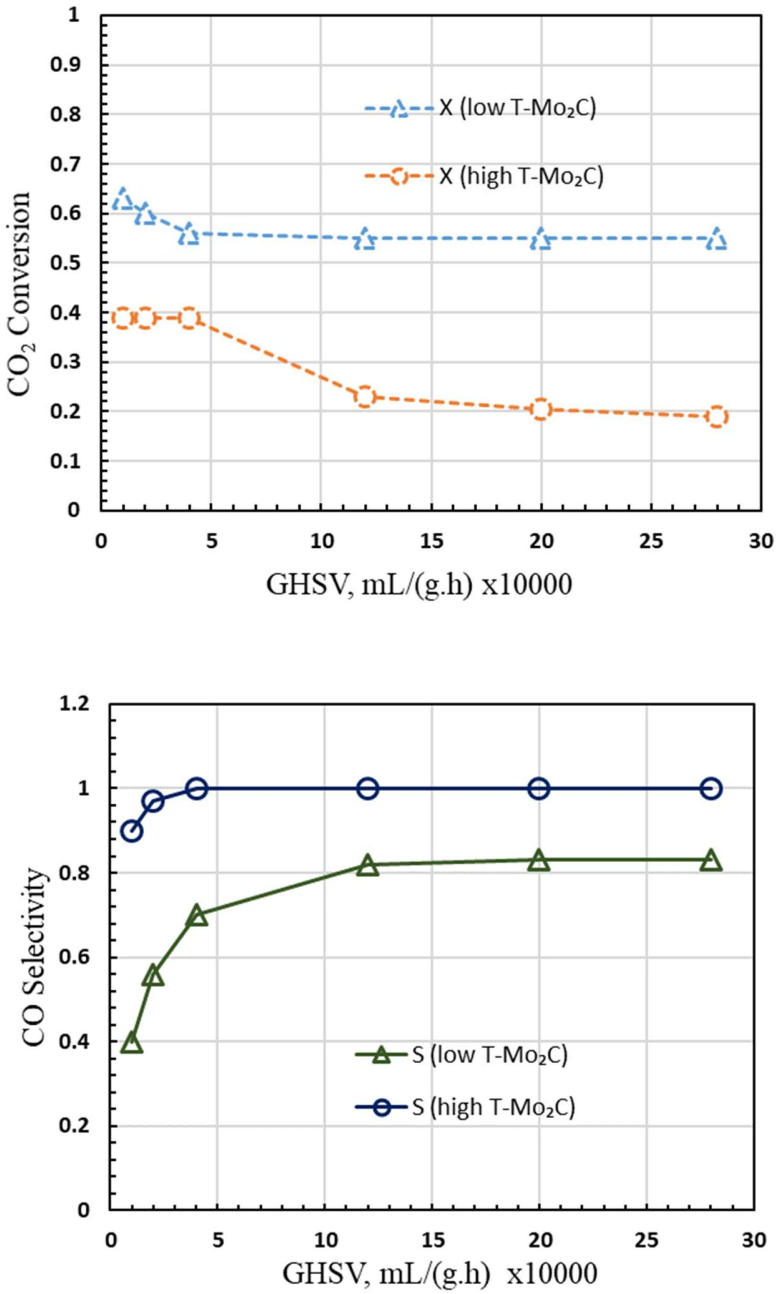

Figure 7: Performance of low T-Mo_2C and high T-Mo_2C at varying GHSV T=450°C, P=30 psi, H_2:CO_2=4

The performance of the two catalysts were also tested as a function of GHSV. As expected, the conversion decreased for both catalysts with increasing GHSV with the conversion dropping more significantly for the high T-Mo_2C. The highest conversion achieved is 62% and 40% for high T- Mo_2C and low T- Mo_2C respectively. The low T-Mo_2C performance remained stable between 120,000-280,000 ml/(g h) GHSV at a conversion of around 55%. The selectivity of both catalysts showed an increasing trend towards the RWGS reaction with increasing GHSV. The low T-Mo_2C showed a significant change in selectivity from 60% towards the Sabatier reaction at GHSV of 10,000 ml/(g h) to 82% selectivity towards the RWGS reaction at a GHSV of 280,000 ml/(g h).

4.1.4 Comparison between supported and bulk Mo_2C

The performance of the supported Mo_2C prepared by using low temperature carburization and high temperature carburization are shown in Figs 7, 8 and Fig. 9, respectively. The performance showed a similar trend in terms of overall conversion with low temperature carburized samples having higher overall conversion with decreased selectivity towards the RWGS reaction. The drop in performance of supported catalyst was within 5% at 500°C at a GHSV of 100,000 ml/(g h) and pressure of 30 psi. The performance of low T-Mo_2C/γ-Al_2O_3 versus varying GHSV was very similar to the performance of bulk low T-Mo_2C. A similar trend was also observed for the high T-Mo_2C/γ-Al_2O_3 and bulk high T-Mo_2C. The high T-Mo_2C/γ-Al_2O_3 showed complete selectivity to RWGS at all GHSV tested whereas the bulk high T-Mo_2C produced small quantities of CH_4 at low GHSV. The results indicate the carburization temperature and mixture has a significant influence on the performance of the catalyst.

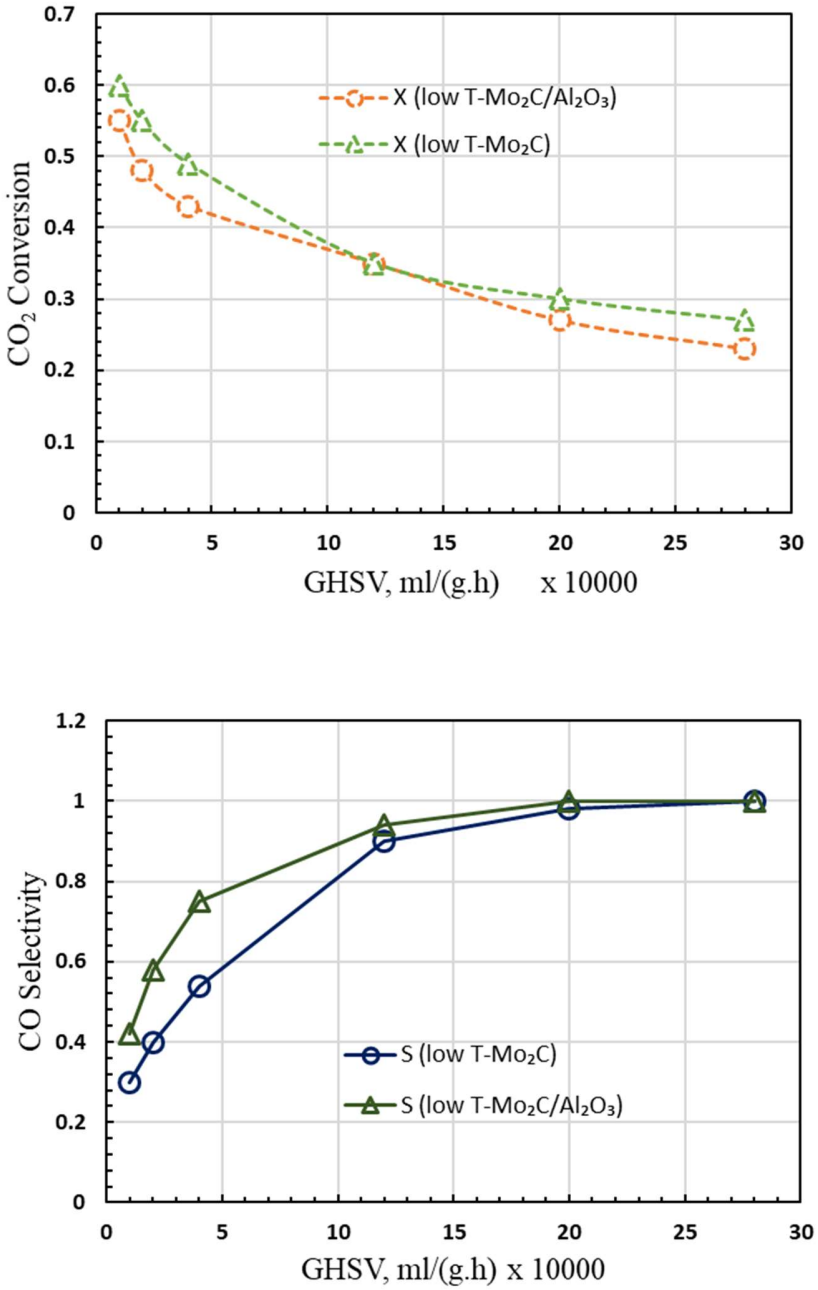

Figure 8: Comparison between supported and bulk low T-Mo_2C for different GHSV, T=450°C, P=30 psi, H_2:CO_2=4

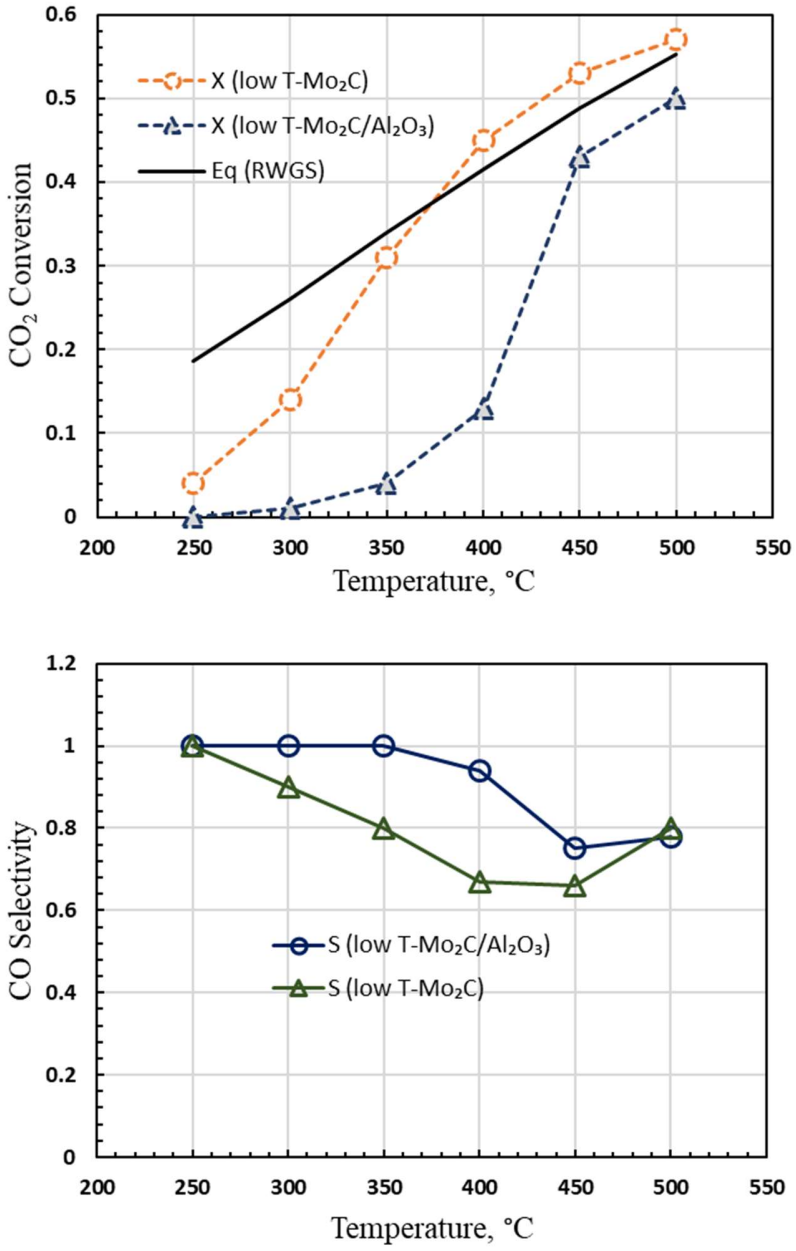

Figure 9: Comparison between high T-Mo_2C and supported high T-Mo_2C, (a): T=450°C, P=30 psi, H_2:CO_2=4, (b): GHSV=100,000 ml/(g h), P =30 psi, H_2:CO_2

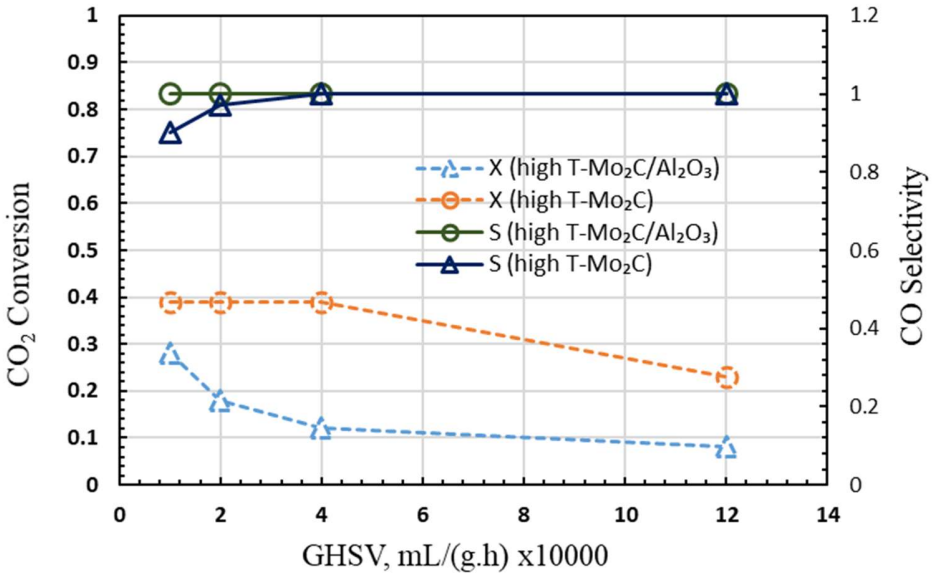

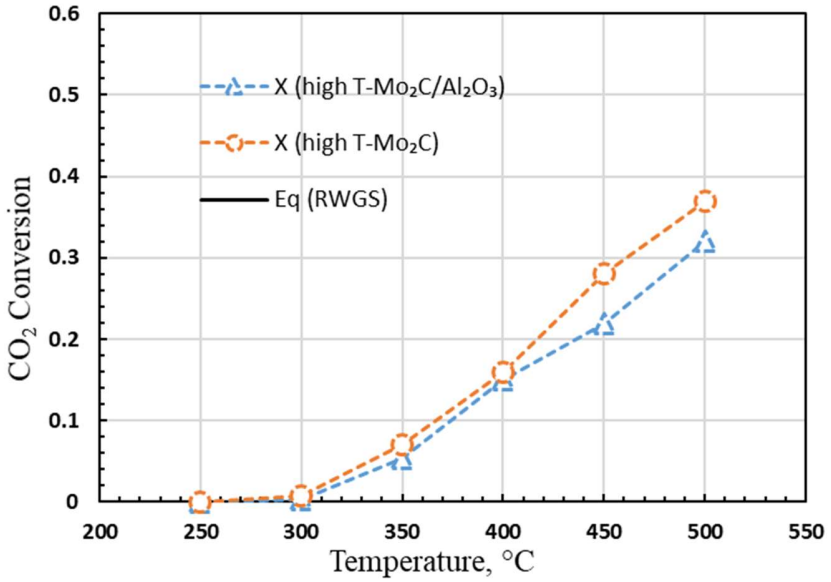

Figure 10: Comparison between high T-Mo_2C and supported high T-Mo_2C, (a): T=450°C, P=30 psi, H_2:CO_2=4, (b): GHSV=100,000 ml/(g h), P =30 psi, H_2:CO_2=4

4.1.5 Stability test of the catalyst

Reports on the stability of Mo_2C and MoO_3 for the RWGS reaction are lacking in the literature. Catalysts are often deactivated due to coking and sintering when operated at elevated temperatures and at industrially relevant operating conditions, i.e., high GHSV. In order to better understand the stability of molybdenum catalysts, tests were performed on supported Mo_2C and MoO_3. The stability test was run at 800°C for supported high T-Mo_2C and supported MoO_3 at GHSV of 100,000 ml/ (g h), 30 psi and H_2:CO_2=4. The initial conversion of the supported Mo_2C catalyst was around 73% with catalyst performance dropping close 71% after 42 h on stream.

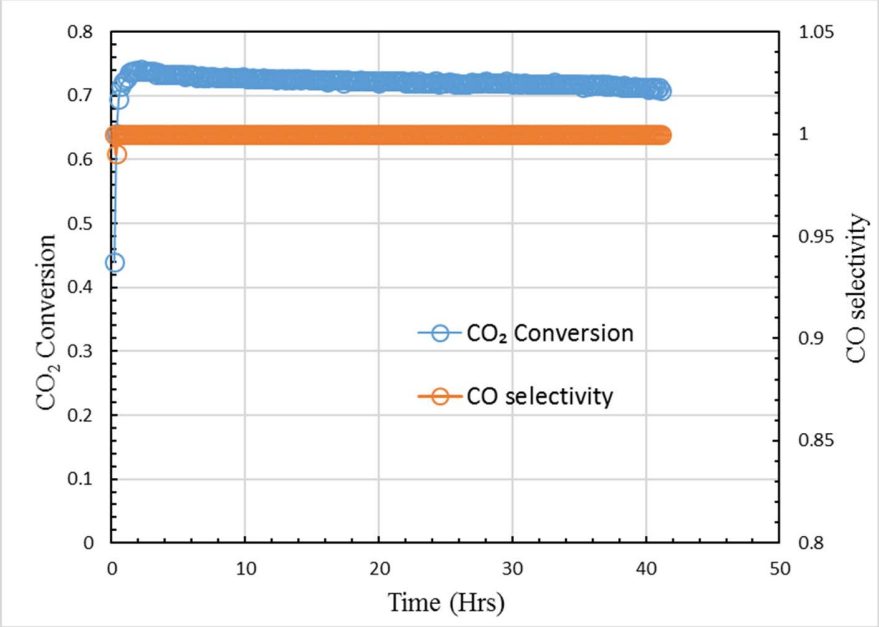

Figure 11: Stability test on high T-Mo_2C/γ-Al_2O_3, GSHV=100,000 ml/(g h), P=30 psi, H_2:CO_2=4 and T=800°C

The selectivity of the supported catalyst remained at 100% to the RWGS reaction through the entire time period of testing. The supported MoO_3 showed decent stability for

the RWGS reaction with initial CO_2 conversions of 75% with performance dropping to 74% after 36 h on stream. Beyond 36 h the reactor begins to plug due to coke formation on the catalyst. To better understand the changes occurring on the catalyst, TGA-MS were conducted on the spent catalysts to see if there is significant coke formation.

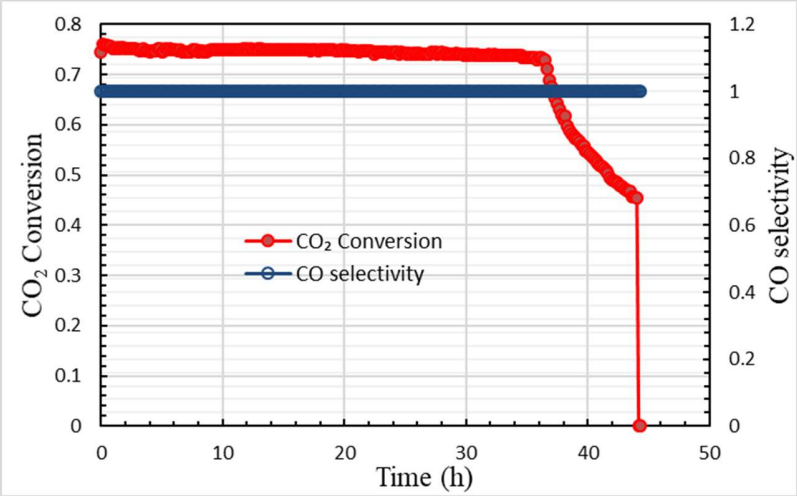

Figure 12: Stability test on MoO_3/γ-Al_2O_3, GSHV=100,000 ml/(g h), P=30 psi, H_2:CO_2=4 and T=800°C

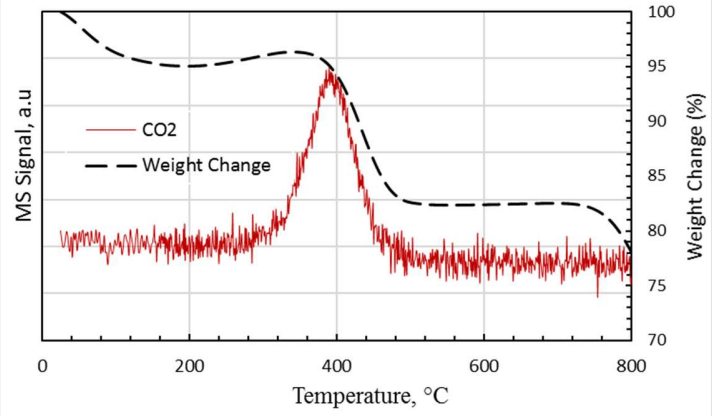

Figure 13: TGA-MS of spent Mo_2C/γ-Al_2O_3 catalyst ran at 800°C, temperature ramping rate was 10°C/min for T ≤ 150°C and 2°C/min for T = 150-800°C. Air flow rate was 40 ml/min.

The $Mo_2C/\gamma\text{-}Al_2O_3$ catalyst showed an initial weight loss in the 20-200°C range. This initial weight loss of around 5% is caused due to the evaporation of absorbed water from the sample below 200°C. In the 200-380°C range, the sample showed mild weight gain of around 2%. We hypothesize the mild gain may be surface oxidation of sample from Mo_2C to MoO_3, with the bulk of the catalyst still remaining a carbide. This could possibly explain the release of CO_2 gas along with the increase in weight of the sample that occurs in the 200-380°C range.

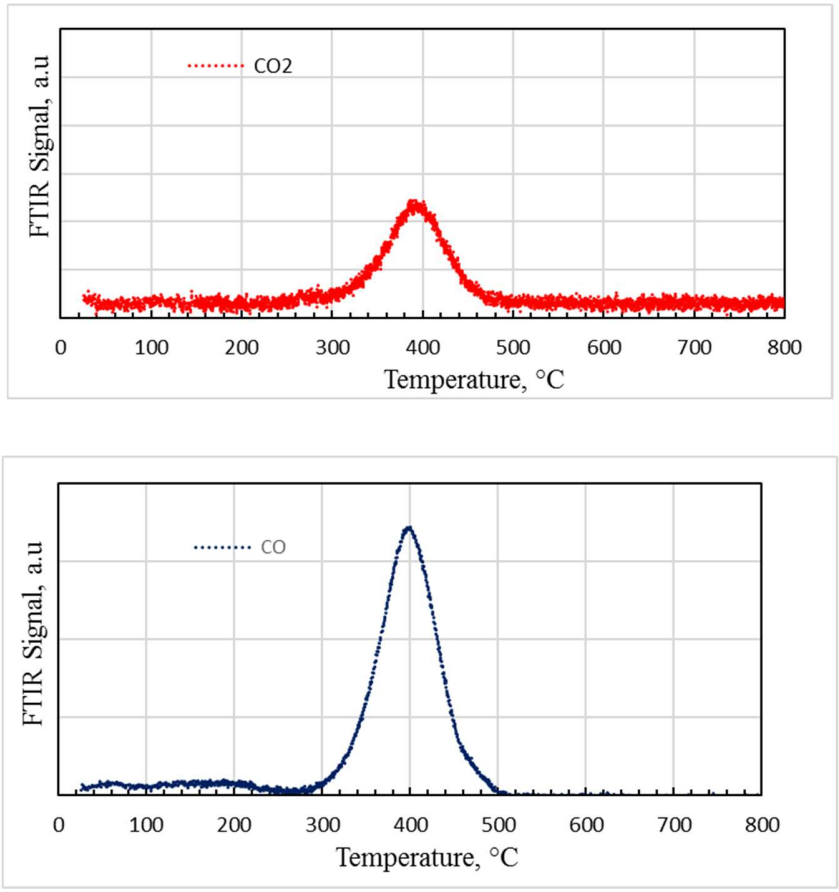

Figure 14: FTIR data of TGA-MS of spent $Mo_2C/\gamma\text{-}Al_2O_3$ catalyst ran at 800°C, temperature ramping rate was 10°C/min for T ≤ 150°C and 2°C/min for T = 150-800°C. Air flow rate was 40 ml/min.

At temperatures above 380°C the sample undergoes a sharp drop in weight, coinciding with a CO_2 peak at 400°C. The CO_2 peak at 400°C is attributed to the oxidation of the deposited carbon on the surface. The results are reconfirmed using the FTIR measurements which showed presence of both CO_2 and CO peaks at 400°C. However, the deposited carbon on the surface of the catalyst did not seem to affect the performance of the catalyst during the stability test. This observation indicates that the extent of coking on the catalyst surface was relatively small, not enough to deactivate the catalyst.

TGA-MS was also conducted on spent $MoO_3/\gamma\text{-}Al_2O_3$ catalyst. The catalyst showed a similar weight loss trend initially below 300°C due to evaporation of adsorbed water on the surface. Beyond 300°C the catalyst had a weight increase due to the Oxidation of $MoO_2/\gamma\text{-}Al_2O_3$ formed on the surface during the reaction back to $MoO_3/\gamma\text{-}Al_2O_3$. There is a sharp CO_2 peak at 650°C and a corresponding weight drop at this temperature due to oxidation of surface carbon to CO_2.

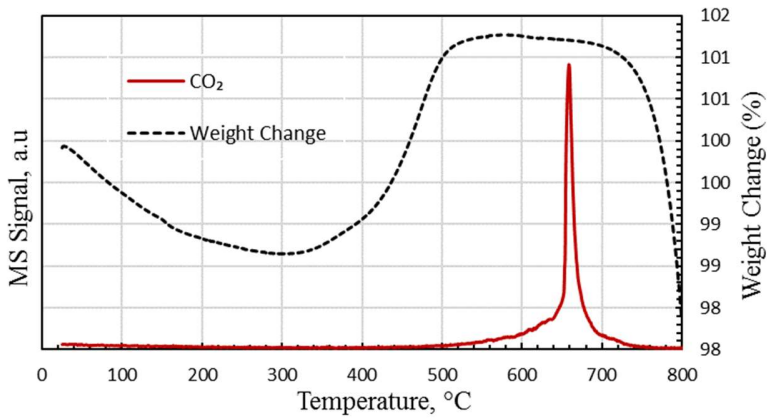

Figure 15: TGA-MS of spent $MoO_3/\gamma\text{-}Al_2O_3$ catalyst ran at 800°C, temperature ramping rate was 10°C/min for T ≤ 150°C and 2°C/min for T = 150-800°C. Air flow rate was 40 ml/min.

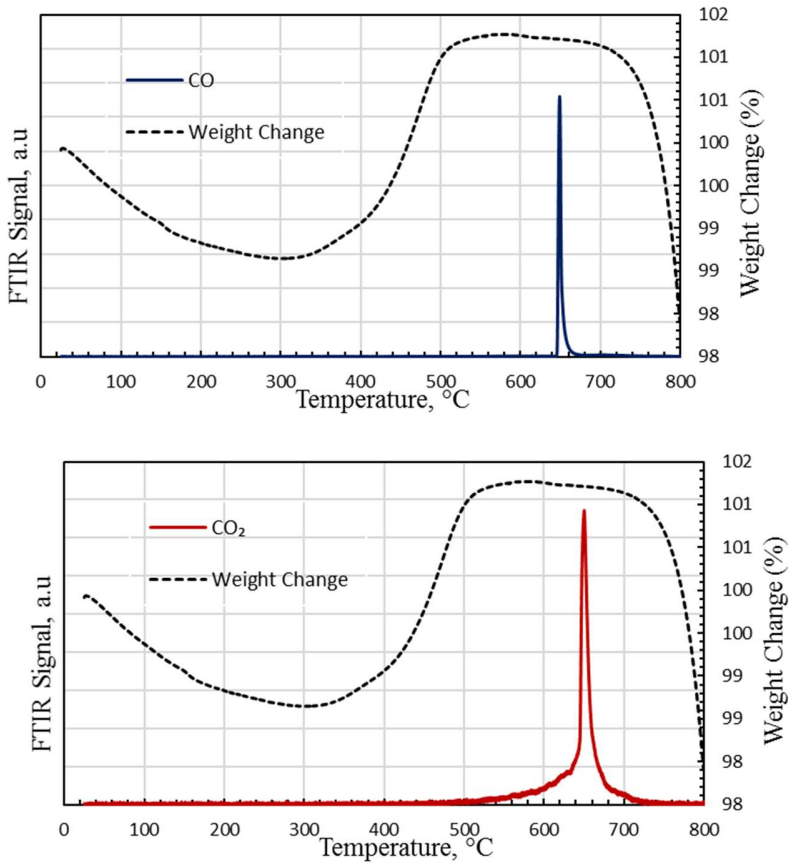

Figure 16: FTIR data of TGA-MS of spent $MoO_3/\gamma\text{-}Al_2O_3$ catalyst ran at 800°C, temperature ramping rate was 10°C/min for T ≤ 150°C and 2°C/min for T = 150-800°C. Air flow rate was 40 ml/min.

The results are reconfirmed using the FTIR measurement, which showed peak of CO_2 and CO at 650°C. The deposited carbon the surface of the $MoO_3/\gamma\text{-}Al_2O_3$ seem to be more stable and are oxidized at higher temperatures which might explain the faster coking and deactivation process of this catalyst. A possible explanation for the better activity of $Mo_2C/\gamma\text{-}Al_2O_3$ is the carbon being formed on the surface is consumed partially consumed during the reaction process as it reacts with hydrogen or oxygen present on the surface at lower temperatures.

4.2 Sabatier reaction

4.2.1 Effect of carburization conditions on $Co_2C/\gamma\text{-}Al_2O_3$ as compared to $CoO_x/\gamma\text{-}Al_2O_3$

The performance of 22% $Co_2C/\gamma\text{-}Al_2O_3$ carburized using a CH_4/H_2 mixture at 800°C and in an ethane/hydrogen mixture at 650°C are shown in Figs 17, 18 22% $Co_2C/\gamma\text{-}Al_2O_3$ carburized in an ethane/hydrogen mixture showed higher selectivity towards the Sabatier reaction at all temperatures tested. The conversion increased exponentially beyond 300°C for high T-$Co_2C/\gamma\text{-}Al_2O_3$ and above 250°C for low T-$Co_2C/\gamma\text{-}Al_2O_3$. The maximum conversion recorded were 67% and 80% for the high T $Co_2C/\gamma\text{-}Al_2O_3$ and low T-$Co_2C/\gamma\text{-}Al_2O_3$ respectively at 500°C, GHSV= 40,000 ml/(g h) and 30 psi.

The performance of the $CoO_x/\gamma\text{-}Al_2O_3$, Fig. 17, showed a similar trend to the high T-$Co_2C/\gamma\text{-}Al_2O_3$ with conversion increasing exponentially above 300°C. The maximum conversion achieved by the $CoO_x/\gamma\text{-}Al_2O_3$ was 57% with selectivity increasing with temperature similar to the high T-$Co_2C/\gamma\text{-}Al_2O_3$. The 25.4 % $CoO_x/\gamma\text{-}Al_2O_3$ had superior performance to the high T-Co_2C at lower temperatures although conversion seems to plateau around 500°C. The low T-$Co_2C/\gamma\text{-}Al_2O_3$ outperforms both catalyst with higher conversion and selectivity towards the Sabatier reaction at all temperatures tested.

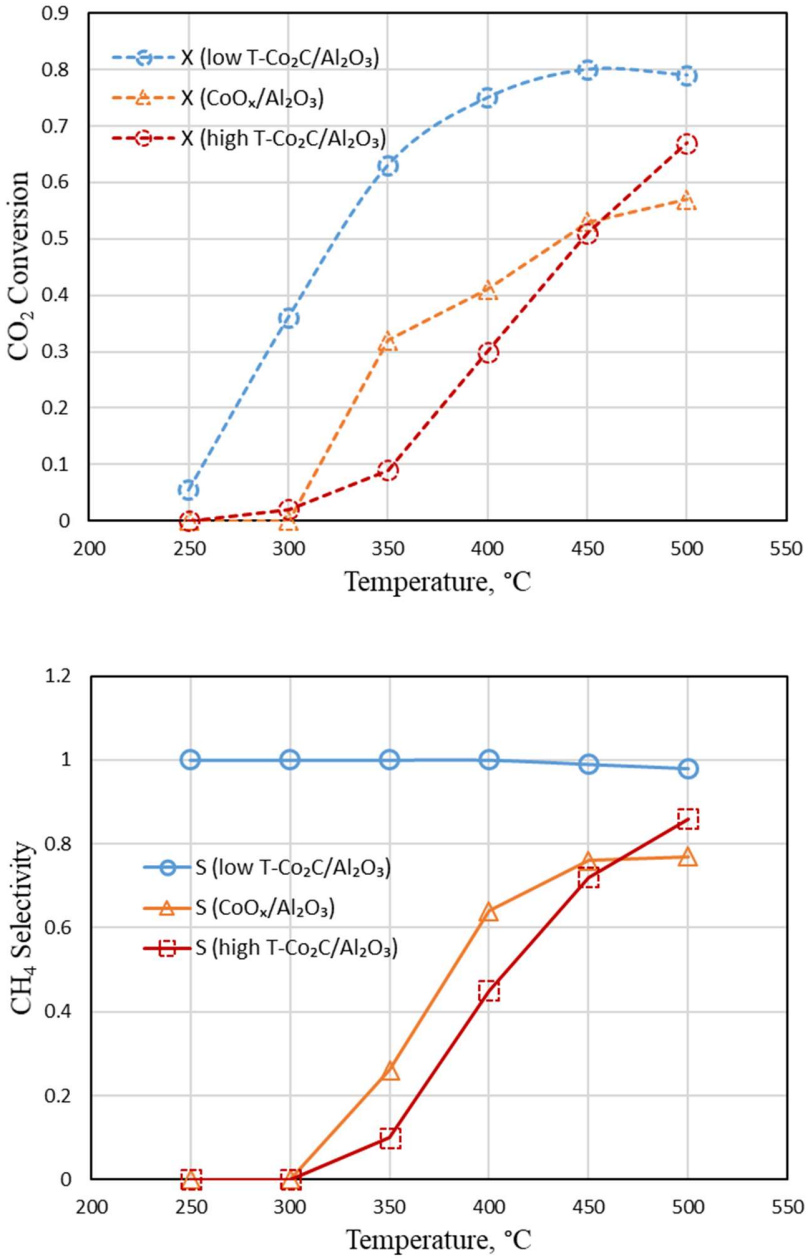

Figure 17: CO_2 conversion and CH_4 selectivity as a function of temperature. Reaction condition: T=250-500°C, GHSV=40,000 ml/(g h), H_2:CO_2=4, P=30 psi

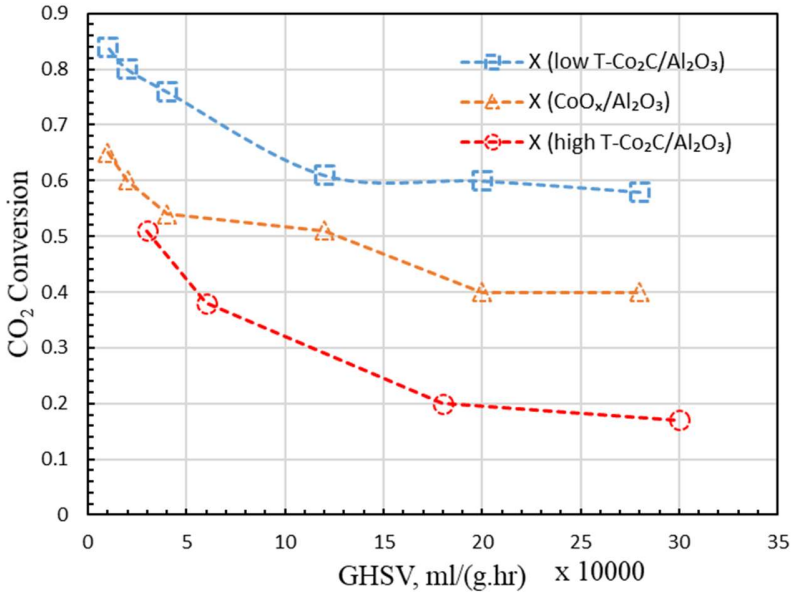

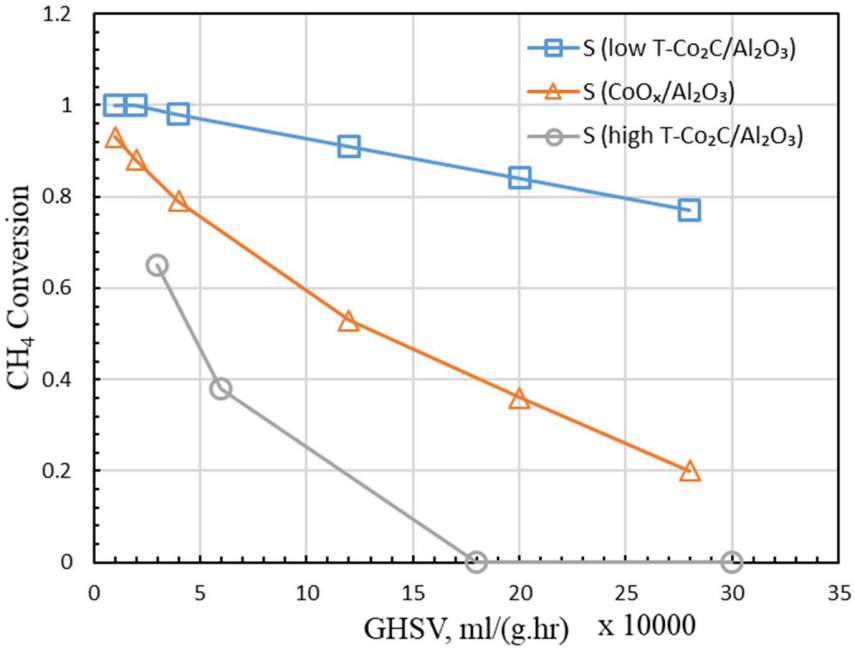

Figure 18: CO_2 conversion and CH_4 selectivity as a function of temperature. Reaction condition: T=450°C, GHSV=10,000-300,000 ml/(g h), H_2:CO_2=4, P=30 psi.

CO_2 conversion and CH_4 selectivity as a function of GHSV are shown in Fig. 18. The effect of carburization temperature and mixture used is more clearly visible when performance was tested as function of GHSV with low T-Co_2C/γ-Al_2O_3 having significantly better conversion and selectivity than the other two catalysts. At the lowest GHSV tested low T-Co_2C/γ-Al_2O_3 catalyst showed complete selectivity towards the Sabatier reaction with CoO_x/γ-Al_2O_3 showing around 93% selectivity towards the Sabatier reaction. The high T-Co_2C/γ-Al_2O_3 had a lower performance than the CoO_x/γ-Al_2O_3 with selectivity towards the Sabatier reaction decreasing more sharply than the other two catalysts tested.

At a GHSV of 180,000 ml/(g h) the high T-Co_2C/γ-Al_2O_3 showed no selectivity towards the methanation reaction although the catalyst still showed 20% CO_2 conversion through the RWGS reaction. The conversion on low T-Co_2C/γ-Al_2O_3 begins to level out around a GHSV of 120,000 ml/(g h) with no significant drop seen until a GHSV of 280,000 ml/(g h) although selectivity continues to drop for the Sabatier reaction. A similar trend is seen for the CoO_x/γ-Al_2O_3 catalyst around 200,000 ml/(g h) to 280,000 ml/(g h) and high T-Co_2C/γ-Al_2O_3 from 180,000 ml/(g h) to 300,000 ml/(g h).

The carburization of CoO_x/γ-Al_2O_3 using CH_4 at a temperature of 800°C seems to deactivate the catalyst towards the Sabatier reaction at temperatures below 450°C, whereas the low temperature carburization process has a promoting effect on the overall performance of the catalyst. Further analyzes needs to be done to understand the structural changes occurring during the carburization process to understand the variation in performance.

4.3 Stability tests

The stability tests on low T-Co_2C/γ-Al_2O_3 were performed at a temperature of 450°C, H_2:CO_2=4, P=30 psi, and GHSV of 40,000 ml/(g h). The results of the stability test performed on low T-Co_2C/γ-Al_2O_3 are shown in Fig. 19. The catalyst did not show any significant deactivation after 65 h on stream. The selectivity towards the Sabatier reaction also remained stable during the deactivation test. The CO_2 conversion at the beginning of the beginning of the test was around 85% with conversion dropping to 84% after 64 h on stream.

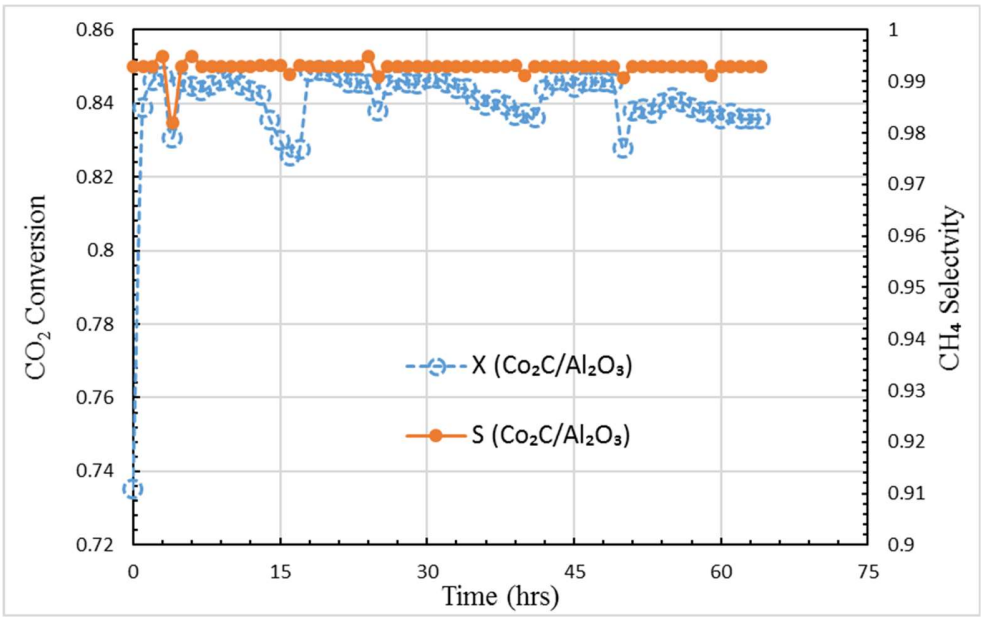

Figure 19: Stability test on low T-Co_2C/γ-Al_2O_3. Reaction conditions: P=30 psi, T=450°C, GHSV=40,000 ml/(g h), H_2:CO_2=4.

The spent catalyst was then analyzed using TGA-MS, to investigate the extent of coke formation. The catalyst showed an initial weigh loss below 200°C due to evaporation of water from the surface. Similarly to Mo_2C, there is sharp CO_2 peak at 400°C. There is also

an additional peak at 500°C. The oxidation of carbon deposited at 400°C does not have a significant change on the overall weight of the catalyst with less than 3% overall drop in weight between 200-400°C. This could be as result of the two competing processes occurring at the same. Weight loss due to oxidation of carbon on the surface and weight gain due to the oxidation of low T-Co_2C/γ-Al_2O_3 to form CoO_x/γ-Al_2O_3 at 400°C. The peak at 500°C coincides with a sharp drop in overall weight of the sample with a 17% drop in overall weight from 400-800°C. Despite the extent of carbon deposition found on the catalytic material, catalytic activity of the material had less than a 1% drop in CO_2 conversion.

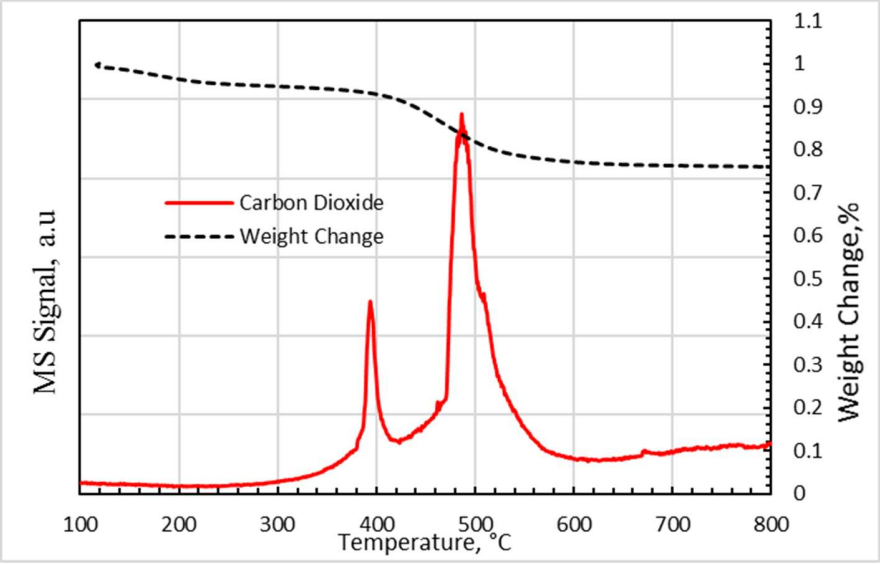

Figure 20 TGA-MS of spent Co_2C, temperature ramping rate was 10°C/min for T ≤ 150°C and 2°C/min for T= 150-800°C. Air flow rate was 40 ml/min.

Chapter 5

Characterization results

5.1 Molybdenum carbide catalysts

The catalyst composition was verified using ICP-MS. The composition did not vary significantly from the target compositions of 21.25 wt% Mo_2C with composition ranging from 19.8%-20.5%. Mo_2C and MoO_3 were characterized by XRD, SEM-EDS and TPR, to understand the structure, morphology and mechanism involved in the reactions.

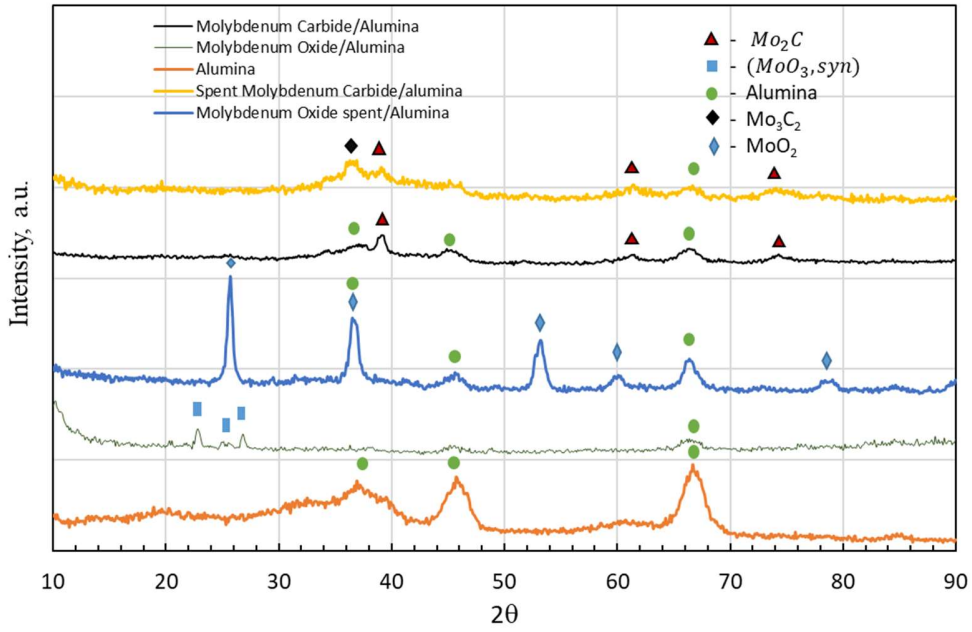

Figure 21: XRD patterns of supported molybdenum catalysts and γ-Al_2O_3

XRD patterns of fresh and spent catalysts supported on γ-Al_2O_3 are shown in Fig. 17. The characteristic peaks corresponding to Mo_2C where identified at 2θ=39.3, 61.6, and 74.8° as expected. The spent Mo_2C/γ-Al_2O_3 catalyst also showed an additional peaks of

Mo_3C_2 at 2θ=36.5°. γ-Al_2O_3 peaks were also identified at 2θ= 36.9, 45.7, and 66.7° in the Mo_2C/γ-Al_2O_3.

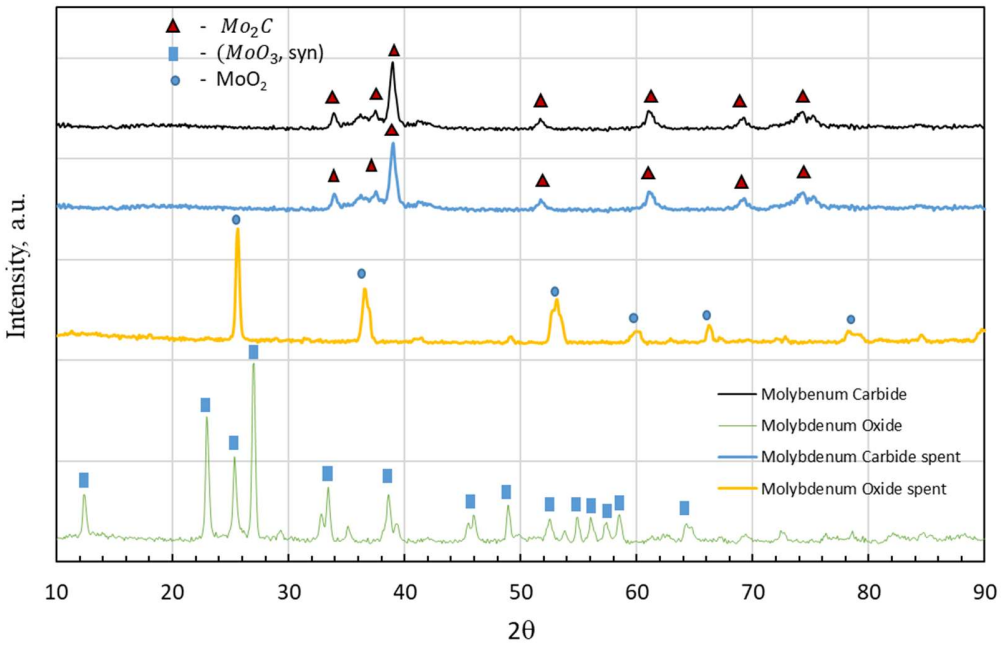

Figure 22 XRD patterns of bulk molybdenum catalysts

The characteristic peaks corresponding to MoO_3 were identified for the fresh supported catalyst at 2θ=23.3, 25.7, and 27.3°. The supported MoO_3 after reaction seems to undergo reduction to form MoO_2 whose peaks were identified at 2θ=26.0, 37.0, 53.5, 61.1, and 79.0°. Similar results were seen for the bulk catalyst with Mo_2C showing peaks at 2θ=34.4, 38.0, 39.4, 61.5, 69.6, 74.6, 34.4, 37.8, 39.3, 61.6, 69.5, and 74.8°. The spent Mo_2C did not however show peaks corresponding to Mo_3C_2 which was seen in the supported Mo_2C after reaction.

Bulk MoO_3 shows peaks associated with it at 2θ=23.3, 25.7, 27.3, and 39.0°. Similar to the supported MoO_3, the spent MoO_3 undergoes reduction during the reaction to form MoO_2 with characteristic peaks being identified at 2θ=26.0, 37.0, 53.5, 61.1, and 79.0°.

Table 1: BET surface area of tested catalysts.

Catalyst	BET surface area m^2/g
MoO_3	4.65
Mo_2C	15.34
Commercial Al_2O_3	206
20% MoO_3 /Al_2O_3	126.51
Mo_2C/ Al_2O_3	99.45

BET surface area was calculated and measured for all catalyst. The bulk MoO_3 undergoes an increase in surface after the carburization process. The catalyst surface area drops after the impregnation and calcination step to from MoO_3/γ-Al_2O_3. The BET surface area of decreases after impregnation for the supported catalyst with the surface area further dropping after the carburization process. No increase in surface area was seen for the supported catalyst after carburization this could possibly be caused by the blocking of Al_2O_3 pores during the carburization step.

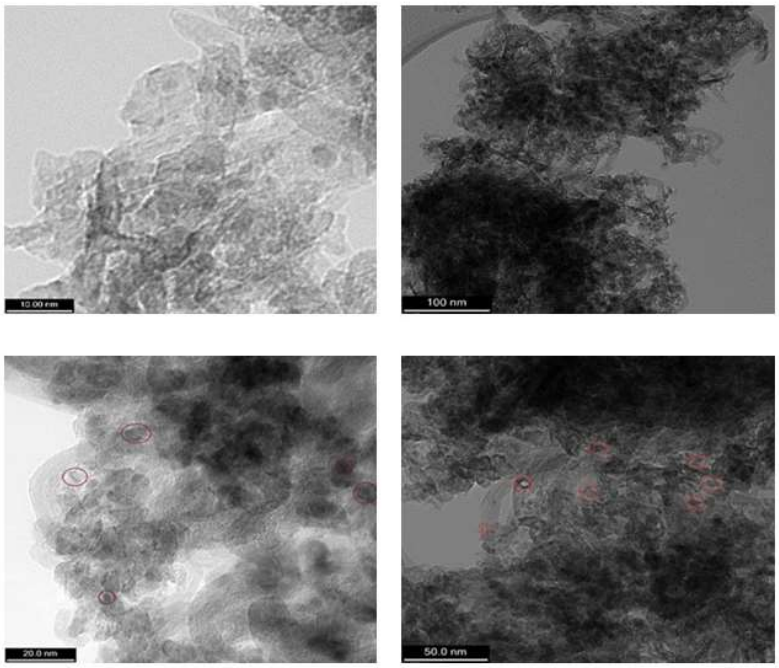

Figure 23: TEM images of $Mo_2C/\gamma\text{-}Al_2O_3$.

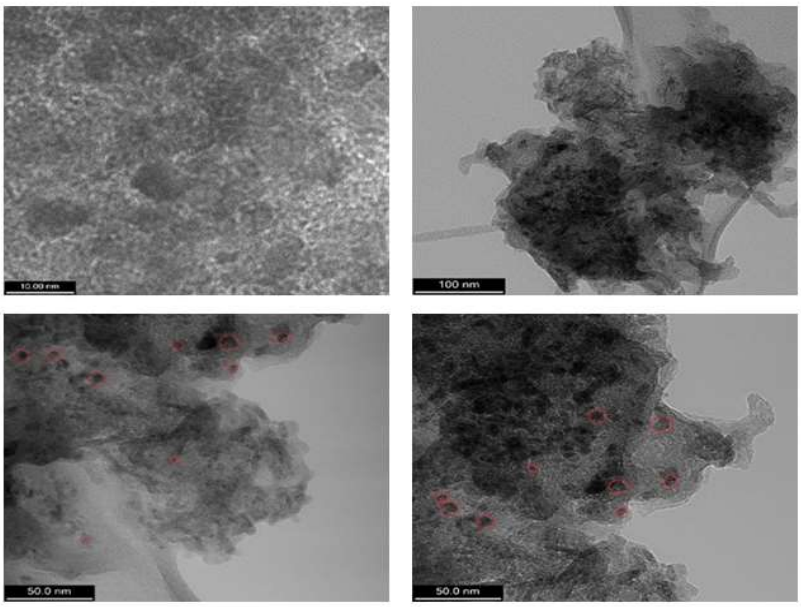

Figure 24: TEM images of spent $Mo_2C/\gamma\text{-}Al_2O_3$.

TEM images were used to calculate particle size distribution, dispersion and turnover frequencies on the catalyst. $Mo_2C/\gamma\text{-}Al_2O_3$ particles sizes ranged from 3-27 nm with average particle sizes in the range of 7 nm. The spent $Mo_2C/\gamma\text{-}Al_2O_3$ particles sizes ranged from 3-20 nm with average particle size of 8 nm.

Table 2: BET surface area, particle diameter, dispersion and TOF of $Mo_2C/\gamma\text{-}Al_2O_3$

Catalyst	BET surface area (m^2/g)	Diameter (nm) ±STD	Dispersion	TOF, s^{-1}
fresh	99.45	6.8 ± 3.3	0.363	1.2821
spent		8.4 ± 3.0	0.357	1.306

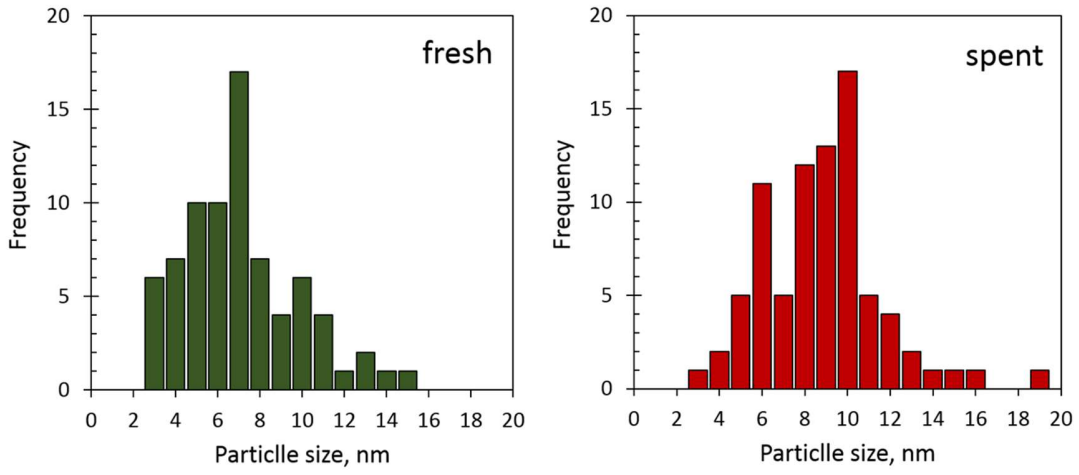

Figure 25: PSD for $Mo_2C/\gamma\text{-}Al_2O_3$ calculated using TEM images.

Turn over frequency (TOF) is defined as the specific activity of an active site per unit time and can be used to evaluate the overall catalytic activity of a catalyst. To calculate TOF, active phase dispersion D and CO_2 conversion rate per unit weight of active phase at high GHSV R_{max} were needed. Active phase dispersion was using Eq. (25) and Eq. (11). V_t

is total volume of the active phase in Eq. (11), was calculated considering polydispersity (non-uniform dispersion).

$$D = \frac{1}{V_t} \sum_{i}^{d_{p,\max}} \frac{\pi d_{p,i}^2}{A_{Me}} \frac{6M_{W,Me}}{N_A \rho_{Me} \pi d_{p,i}^3} \frac{\pi d_{p,i}^3}{6} f_i \tag{25}$$

$$V_t = \sum_{i}^{d_{p,\max}} \frac{\pi d_{p,i}^3}{6} f_i \tag{26}$$

Active site diameter $d_{p,i}$ and its fraction f_i were obtained from particle size distribution using TEM pictures. A_{Me} is the surface area occupied by a single active site which was calculated to be 0.05nm^2 using the assumption that 20 molecules occupy one nm^2, N_A is the Avogadro number, ρ_{Me} is the gravimetric density of the active phase, $M_{W,Me}$ is the active phase molecular weight.. Eq. (12) and Eq. (13) was used to calculate CO_2 conversion rate per unit weight of catalyst and CO_2 conversion rate per unit weight of active phase respectively. $F_{CO_2,f}$ is the flow rate of carbon dioxide flowing into the reactor, X_{CO_2} is the carbon dioxide conversion, w_c is the weight of catalyst. L_{Me} is active metal loading in percentage.

$$r = \frac{Q_{CO_2,f} X_{CO_2}}{w_c} \tag{27}$$

$$R = 100 \frac{r}{L_{Me}} \tag{28}$$

By Eq. (29) turnover frequency (TOF) was calculated:

$$TOF = \frac{M_{W,Me}}{D} R_{max} \tag{29}$$

Chapter 6

Conclusion and future work

6.1 Reverse water gas shift reaction

The reverse water gas shift (RWGS) reaction was conducted over unsupported and supported molybdenum oxide (MoO_3) and carbide (Mo_2C). The catalysts were active in RWGS and selective towards CO formation. The Mo_2C catalyst was more selective at all temperatures tested, attaining complete selectivity to CO production.

The supported Mo_2C catalyst (20wt%Mo_2C/γ-Al_2O_3) was more stable than the corresponding molybdenum oxide catalyst (20wt%MoO_3/γ-Al_2O_3). When operated at 800°C and a gas hourly space velocity (GHSV) of 100,000 ml/(g h), conditions which are relevant to industrial operation, the 20wt%MoO_3/γ-Al_2O_3 deactivated because of coking that caused complete clogging after 40 h time-on-stream. For the 20wt%Mo_2C/γ-Al_2O_3 catalyst, although some coke formation was observed, no detectable drop in performance was detected over 50 h time-on-stream.

Changing carburization conditions to a higher hydrocarbon (ethane) and lower temperatures improved the catalytic performance of Mo_2C in terms of activity, although selectivity towards CO formation reduced, particularly at lower space velocities. Further research is required in order to understand the effects of carburization conditions on the Mo_2C catalyst performance.

6.2 Sabatier reaction

The Sabatier reaction was conducted over supported cobalt oxide and carbide catalysts (20wt% $CoO/\gamma\text{-}Al_2O_3$ and 20wt% $Co_2C/\gamma\text{-}Al_2O_3$). Catalytic performance evaluation showed CO_2 conversions up to 85% at 450°C and a GHSV of 40,000 ml/(g h) for the Co_2C catalyst with no detectable deactivation over 60 h time-on-stream. Carburization of cobalt oxide to cobalt carbide significantly improves the catalytic performance of the material with increased selectivity towards CH_4 formation.

The exact reaction mechanism over CoO and Co_2C catalysts is still to be verified and requires more investigation. The carburization mixture composition plays an important role in determining the catalytic performance. High temperature carburization using methane resulted in lower activity as compared to low temperature carburization using ethane. The carburization procedure should be further fine-tuned to optimize catalytic performance.

Reference

[1] Kopetz, H., K. Haara, and B. V. Kummamuru. "WBA global bioenergy statistics 2015. "World Bioenergy Association, http://worldbioenergy.org/uploads/WBA%20Global%20Bioenergy%20Statistics%202015.pdf, Accessed March 18 (2015).

[2] Rochelle, Gary T. "Amine scrubbing for CO_2 capture." Science 325.5948 (2009): 1652-1654.

[3] Shibata, Masami, Kohji Yoshida, and Nagakazu Furuya. "Electrochemical synthesis of urea at gas-diffusion electrodes: Part II. Simultaneous reduction of carbon dioxide and nitrite ions at Cu, Ag and Au catalysts." Journal of Electroanalytical Chemistry 442.1-2 (1998): 67-72.

[4] Kayan, Didem Balun, and Fatih Köleli. "Simultaneous electrocatalytic reduction of dinitrogen and carbon dioxide on conducting polymer electrodes." Applied Catalysis B: Environmental 181 (2016): 88-93.

[5] Simakov, David S.A. Renewable Synthetic Fuels and Chemicals from Carbon Dioxide: Fundamentals, Catalysis, Design Considerations and Technological Challenges. Springer, 2017.

[6] Porosoff, Marc D., Binhang Yan, and Jingguang G. Chen. "Catalytic reduction of CO_2 by H_2 for synthesis of CO, methanol and hydrocarbons: challenges and opportunities." Energy & Environmental Science 9.1 (2016): 62-73.

[7] Wang, Wei, et al. "Recent advances in catalytic hydrogenation of carbon dioxide." Chemical Society Reviews 40.7 (2011): 3703-3727.

[8] Weatherbee, Gordon D., and Calvin H. Bartholomew. "Hydrogenation of CO_2 on group VIII metals: I. Specific activity of $NiSiO_2$." Journal of Catalysis 68.1 (1981): 67-76.

[9] Oshikawa, Katsuhiko, Masatoshi Nagai, and Shinzo Omi. "Characterization of molybdenum carbides for methane reforming by TPR, XRD, and XPS." The Journal of Physical Chemistry B 105.38 (2001): 9124-9131.

[10] Tominaga, Hiroyuki, and Masatoshi Nagai. "Density functional study of carbon dioxide hydrogenation on molybdenum carbide and metal." Applied Catalysis A: General 282.1-2 (2005): 5-13.

[11] Saito, Masahiro, and Robert B. Anderson. "The activity of several molybdenum compounds for the methanation of CO_2." Journal of Catalysis 67.2 (1981): 296-302.

[12] Liu, Ping, and José A. Rodriguez. "Water-gas-shift reaction on molybdenum carbide surfaces: essential role of the oxycarbide." The Journal of Physical Chemistry B 110.39 (2006): 19418-19425.

[13] Schweitzer, Neil M., et al. "High activity carbide supported catalysts for water gas shift." Journal of the American Chemical Society 133.8 (2011): 2378-2381.

[14] Qi, Ke-Zhen, Gui-Chang Wang, and Wen-Jun Zheng. "A first-principles study of CO hydrogenation into methane on molybdenum carbides catalysts." Surface Science 614 (2013): 53-63.

[15] Patterson, Patricia M., Tapan K. Das, and Burtron H. Davis. "Carbon monoxide hydrogenation over molybdenum and tungsten carbides." Applied Catalysis A: General 251.2 (2003): 449-455.

[16] Qi, Ke-Zhen, Gui-Chang Wang, and Wen-Jun Zheng. "A first-principles study of CO hydrogenation into methane on molybdenum carbides catalysts." Surface Science 614 (2013): 53-63.

[17] Moodley, D. J., et al. "Carbon deposition as a deactivation mechanism of cobalt-based Fischer–Tropsch synthesis catalysts under realistic conditions." Applied Catalysis A: General 354.1-2 (2009): 102-110.

[18] Weller, Sol, L. J. E. Hofer, and R. B. Anderson. "The Role of Bulk Cobalt Carbide in the Fischer—Tropsch Synthesis1." Journal of the American Chemical Society 70.2 (1948): 799-801.

[19] Pei, Yan-Peng, et al. "High alcohols synthesis via Fischer–Tropsch reaction at cobalt metal/carbide interface." ACS Catalysis 5.6 (2015): 3620-3624.

[20] Ratnasamy, Chandra, and Jon P. Wagner. "Water gas shift catalysis." Catalysis Reviews 51.3 (2009): 325-440.

[21] Mallapragada, Dharik S., et al. "Sun-to-fuel assessment of routes for fixing CO_2 as liquid fuel." Industrial & Engineering Chemistry Research 52.14 (2013): 5136-5144.

[22] Oshima, Kazumasa, et al. "Low temperature catalytic reverse water gas shift reaction assisted by an electric field." Catalysis Today 232 (2014): 27-32.

[23] Centi, Gabriele, and Siglinda Perathoner. "Opportunities and prospects in the chemical recycling of carbon dioxide to fuels." Catalysis Today 148.3-4 (2009): 191-205.

[24] Kim, Sung Su, Hyun Hee Lee, and Sung Chang Hong. "The effect of the morphological characteristics of TiO_2 supports on the reverse water–gas shift reaction over Pt/TiO_2 catalysts." Applied Catalysis B: Environmental 119 (2012): 100-108.

[25] Pettigrew, D. J., D. L. Trimm, and N. W. Cant. "The effects of rare earth oxides on the reverse water-gas shift reaction on palladium/alumina." Catalysis Letters 28.2-4 (1994): 313-319.

[26] Goguet, Alexandre, et al. "Study of the origin of the deactivation of a Pt/CeO_2 catalyst during reverse water gas shift (RWGS) reaction." Journal of Catalysis 226.2 (2004): 382-392.

[27] Barreiro, M. M., M. Maroño, and J. M. Sánchez. "Hydrogen permeation through a Pd-based membrane and RWGS conversion in H_2/CO_2, $H_2/N_2/CO_2$ and $H_2/H_2O/CO_2$ mixtures." International Journal of Hydrogen Energy 39.9 (2014): 4710-4716.

[28] Toyir, J., et al. "Sustainable process for the production of methanol from CO_2 and H_2 using Cu/ZnO-based multicomponent catalyst." Physics Procedia 2.3 (2009): 1075-1079.

[29] Oshikawa, Katsuhiko, Masatoshi Nagai, and Shinzo Omi. "Characterization of molybdenum carbides for methane reforming by TPR, XRD, and XPS." The Journal of Physical Chemistry B 105.38 (2001): 9124-9131.

[30] Saito, Masahiro, and Robert B. Anderson. "The activity of several molybdenum compounds for the methanation of CO_2." Journal of Catalysis 67.2 (1981): 296-302.

[31] Liu, Ping, and José A. Rodriguez. "Water-gas-shift reaction on molybdenum carbide surfaces: essential role of the oxycarbide." The Journal of Physical Chemistry B 110.39 (2006): 19418-19425.

[32] Schweitzer, Neil M., et al. "High activity carbide supported catalysts for water gas shift." Journal of the American Chemical Society 133.8 (2011): 2378-2381.

[33] Patterson, Patricia M., Tapan K. Das, and Burtron H. Davis. "Carbon monoxide hydrogenation over molybdenum and tungsten carbides." Applied Catalysis A: General 251.2 (2003): 449-455.

[35] Porosoff, Marc D., et al. "Molybdenum carbide as alternative catalysts to precious metals for highly selective reduction of CO_2 to CO." Angewandte Chemie International Edition 53.26 (2014): 6705-6709.

[36] Gao, Jiajian, et al. "Controllable synthesis of α-MoC_{1-x} and β-Mo_2C nanowires for highly selective CO_2 reduction to CO." Catalysis Communications 84 (2016): 147-150.

[37] Yan, Bing, et al. "Enhanced Carbon Dioxide Oxidative Dehydrogenation of 1-Butene by Iron-Doped Ordered Mesoporous Alumina." ChemCatChem 9.24 (2017): 4480-4483.

[38] Ernst, Karl-Heinz, Charles T. Campbell, and Giuliano Moretti. "Kinetics of the reverse water-gas shift reaction over Cu (110)." Journal of Catalysis 134.1 (1992): 66-74.

[39] Fujita, Shin-Ichiro, Masahito Usui, and Nobutsune Takezawa. "Mechanism of the reverse water gas shift reaction over Cu/ZnO catalyst." Journal of Catalysis 134.1 (1992): 220-225.

[40] Hadden, R. A., et al. "The adsorption and decomposition of carbon dioxide on polycrystalline copper." Catalysis letters 1.1-3 (1988): 27-33.

[42] Salmi, T, and R. Hakkarainen. "Kinetic study of the low-temperature water-gas shift reaction over a Cu-ZnO catalyst." Applied catalysis 49.2 (1989): 285-306.

[41] Chen, Ching-Shiun, and Wu-Hsun Cheng. "Study on the Mechanism of CO Formation in Reverse Water Gas Shift Reaction over Cu/SiO_2 Catalyst by Pulse Reaction, TPD and TPR." Catalysis Letters 83.3-4 (2002): 121-126.

[42] Pour, Ali Nakhaei, et al. "Kinetics of the water-gas shift reaction in Fischer-Tropsch synthesis over a nano-structured iron catalyst." Journal of Natural Gas Chemistry 19.4 (2010): 362-368.

[43] Ortelli, Enrico E., Johanna M. Weigel, and A. Wokaun. "Methanol synthesis pathway over Cu/ZrO_2 catalysts: a time-resolved DRIFT 13 C-labelling experiment." Catalysis Letters 54.1-2 (1998): 41-48.

[44] Arunajatesan, V., et al. "In situ FTIR investigations of reverse water gas shift reaction activity at supercritical conditions." Chemical Engineering Science 62.18-20 (2007): 5062-5069.

[45] Goguet, A., et al. "Pulse-response TAP studies of the reverse water–gas shift reaction over a Pt/CeO_2 catalyst." Journal of Catalysis 237.1 (2006): 102-110.

[46] Sabatier, Paul. "New synthesis of methane." Comptes Rendus 134 (1902): 514-516.

[47] Zhuang, Yichen. Renewable Syngas Generation and Biogas/Landfill Gas Upgrade via Thermocatalytic Conversion of Carbon Dioxide. MS thesis. University of Waterloo, 2017.

[48] Schiebahn, Sebastian, et al. "Power to gas: Technological overview, systems analysis and economic assessment for a case study in Germany." International Journal of Hydrogen Energy 40.12 (2015): 4285-4294.

[49] Murdoch, Karen, et al. "Sabatier methanation reactor for space exploration." 1st Space Exploration Conference: Continuing the Voyage of Discovery. 2005.

[50] Kleiner, G. N., and R. J. Cusick. "Development of an advanced Sabatier CO_2 reduction subsystem." (1981).

[51] Sun, Duo, Faisal Mohamed Khan, and David SA Simakov. "Heat removal and catalyst deactivation in a Sabatier reactor for chemical fixation of CO_2: Simulation-based analysis." Chemical Engineering Journal 329 (2017): 165-177.

[52] Bligaard, T., et al. "The Brønsted–Evans–Polanyi relation and the volcano curve in heterogeneous catalysis." Journal of Catalysis 224.1 (2004): 206-217.

[53] Garbarino, Gabriella, et al. "Methanation of carbon dioxide on Ru/Al_2O_3 and Ni/Al_2O_3 catalysts at atmospheric pressure: Catalysts activation, behaviour and stability." International Journal of Hydrogen Energy 40.30 (2015): 9171-9182.

[54] Kester, Keith B., Ercument Zagli, and John L. Falconer. "Methanation of carbon monoxide and carbon dioxide on Ni/Al2O3 catalysts: effects of nickel loading." Applied Catalysis 22.2 (1986): 311-319.

[55] Cai, Mengdie, et al. "Methanation of carbon dioxide on Ni/ZrO_2-Al_2O_3 catalysts: Effects of ZrO_2 promoter and preparation method of novel ZrO2-Al2O3 carrier." Journal of Natural Gas Chemistry 20.3 (2011): 318-324.

[56] Weatherbee, Gordon D., and Calvin H. Bartholomew. "Hydrogenation of CO_2 on group VIII metals: IV. Specific activities and selectivities of silica-supported Co, Fe, and Ru." Journal of Catalysis 87.2 (1984): 352-362.

[57] Takezawa, Nobutsune, et al. "Methanation of carbon dioxide: Preparation of Ni/MgO catalysts and their performance." Applied Catalysis 23.2 (1986): 291-298.

[58] Bartholomew, Calvin. "Catalyst deactivation and regeneration." Kirk-Othmer Encyclopedia of Chemical Technology (2003).

[59] Dalla Betta, R. A., A. G. Piken, and M. Shelef. "Heterogeneous methanation: Steady-state rate of CO hydrogenation on supported ruthenium, nickel and rhenium." Journal of Catalysis 40.2 (1975): 173-183.

[60] Agnelli, M., M. Kolb, and C. Mirodatos. "CO hydrogenation on a nickel catalyst.: 1. kinetics and modeling of a low-temperature sintering process." Journal of Catalysis 148.1 (1994): 9-21.

[61] Pedernera, Marisa N., Juliana Piña, and Daniel O. Borio. "Kinetic evaluation of carbon formation in a membrane reactor for methane reforming." Chemical Engineering Journal 134.1-3 (2007): 138-144.

[62] Abe, Takayuki, et al. "CO_2 methanation property of Ru nanoparticle-loaded TiO_2 prepared by a polygonal barrel-sputtering method." Energy & Environmental Science 2.3 (2009): 315-321.

[63] Kwak, Ja Hun, Libor Kovarik, and János Szanyi. "CO_2 reduction on supported Ru/Al_2O_3 catalysts: cluster size dependence of product selectivity." ACS Catalysis 3.11 (2013): 2449-2455.

[64] Gao, Jiajian, et al. "Recent advances in methanation catalysts for the production of synthetic natural gas." RSC Advances 5.29 (2015): 22759-22776.

[65] Shen, Wen-Jie, et al. "The influence of the support on the activity and selectivity of Pd in CO hydrogenation." Applied Catalysis A: General 213.2 (2001): 225-232.

[66] Vannice, M. Albert, C. C. Twu, and S. H. Moon. "SMSI effects on CO adsorption and hydrogenation on Pt catalysts: I. Infrared spectra of adsorbed CO prior to and during reaction conditions." Journal of Catalysis 79.1 (1983): 70-80.

[67] Solymosi, Frigyes, and András Erdőhelyi. "Hydrogenation of CO_2 to CH_4 over alumina-supported noble metals." Journal of Molecular Catalysis 8.4 (1980): 471-474.

[68] Iizuka, Tokio, Yukari Tanaka, and Kozo Tanabe. "Hydrogenation of CO and CO_2 over rhodium catalysts supported on various metal oxides." Journal of Catalysis 76.1 (1982): 1-8.

[69] Moodley, D. J., et al. "Carbon deposition as a deactivation mechanism of cobalt-based Fischer–Tropsch synthesis catalysts under realistic conditions." Applied Catalysis A: General 354.1-2 (2009): 102-110.

[70] Weller, Sol, L. J. E. Hofer, and R. B. Anderson. "The Role of Bulk Cobalt Carbide in the Fischer—Tropsch Synthesis1." Journal of the American Chemical Society 70.2 (1948): 799-801.

[71] Pei, Yan-Peng, et al. "High alcohols synthesis via Fischer–Tropsch reaction at cobalt metal/carbide interface." ACS Catalysis 5.6 (2015): 3620-3624.

[72] Falconer, John L., and A. Ercüment Zağli. "Adsorption and methanation of carbon dioxide on a nickel/silica catalyst." Journal of Catalysis 62.2 (1980): 280-285.

[73] Lapidus, A. L., et al. "The mechanism of carbon dioxide hydrogenation on copper and nickel catalysts." Petroleum Chemistry 47.2 (2007): 75-82.

[74] Fujita, S., et al. "Methanation of carbon monoxide and carbon dioxide over nickel catalyst under the transient state." Reaction Kinetics and Catalysis Letters 33.1 (1987): 179-184.

[75] Schild, Ch, A. Wokaun, and A. Baiker. "On the mechanism of CO and CO_2 hydrogenation reactions on zirconia-supported catalysts: a diffuse reflectance FTIR study: Part II. Surface species on copper/zirconia catalysts: implications for methanoi synthesis selectivity." Journal of Molecular Catalysis 63.2 (1990): 243-254.

[76] Marwood, Michel, Ralf Doepper, and Albert Renken. "In-situ surface and gas phase analysis for kinetic studies under transient conditions The catalytic hydrogenation of CO_2." Applied Catalysis A: General 151.1 (1997): 223-246.

[77] Choe, Sang-Joon, et al. "Adsorbed carbon formation and carbon hydrogenation for CO_2 methanation on the Ni (111) surface: ASED-MO study." Bulletin of the Korean Chemical Society 26.11 (2005): 1682-1688.

[78] Kim, Hyun You, Hyuck Mo Lee, and Jung-Nam Park. "Bifunctional mechanism of CO2 methanation on Pd-MgO/SiO_2 catalyst: independent roles of MgO and Pd on CO_2 methanation." The Journal of Physical Chemistry C 114.15 (2010): 7128-7131.

[79] Simakov, David SA, et al. "Solar thermal catalytic reforming of natural gas: a review on chemistry, catalysis and system design." Catalysis Science & Technology 5.4 (2015): 1991-2016.

[80] Adris, A. M., C. J. Lim, and J. R. Grace. "The fluidized-bed membrane reactor for steam methane reforming: model verification and parametric study." Chemical Engineering Science 52.10 (1997): 1609-1622.